The effects of deforestation on downwind precipitation

C. Braat

TU Delft

The effects of deforestation on downwind precipitation

by

C. Braat

as MSc thesis
at the Delft University of Technology.

Student number:	4313488	
Project duration:	August 1, 2020 – July 23, 2021	
Thesis committee:	dr. ir. R.J. van der Ent,	Water Resources, TU Delft
	dr. ir. J.A.E. ten Veldhuis,	Water Resources, TU Delft
	dr. S.L.M. Lhermitte,	Geoscience & Remote Sensing, TU Delft
	dr. ir. R.W. Hut,	Water Resources, TU Delft

TU Delft

Preface

When I started this research almost exactly one year ago, little did I know about the wondrous world of deforestation, precipitation trends, analysing big datasets and using Google Earth Engine. Still, I feel like I just barely scratched the surface of the possibilities within this interesting and relevant field. Due to the Corona pandemic, writing my thesis became even more an individualistic project, with little contact and interaction with my fellow students. While we almost exclusively met online, I felt highly supported by my supervisors. I would like to thank Stef Lhermitte for his sharp remarks on correlation, causation and noise and for his helpful suggestions on limiting the influence of other factors than deforestation by doing a subregional analysis. I would also like to thank Rolf Hut for joining my committee, stressing the importance of statistics within an explorative research. I am also thankful that Marie-Claire ten Veldhuis joined my committee from her own interest, making time every two weeks to meet and provide useful feedback, both on my research set up as well as on my writing. Lastly I would like to thank my main supervisor and the initiator of this research, Ruud van der Ent. I found it very pleasant to work with him and inspirational to contribute to his field. I hope to build upon the knowledge and skills I gained during this research in the future. I'd like to wish you a pleasant read and I hope you gain new insights.

C. Braat
Delft, July 2021

Contents

List of Figures

Abstract

Protecting forests from agricultural expansion and wildfires while the world population is growing and the climate is warming remains one of the biggest challenges humanity currently faces. While global modelling and regional observation based studies have found significant effects from deforestation on precipitation, leading mostly to drying precipitation trends and shorting rainy seasons, this study represents the first global estimate of first order deforestation effects on precipitation. Using a recently developed precipitationshed database and actual deforestation data, a new measure is developed to quantify potential deforestation impact per grid cell which in turn is related to annual precipitation trends as well as seasonal differences in tropical regions. In seven regions analysed, a majority of subregions suggested a relationship between deforestation impact and a relative drying precipitation trend in the 2001-2018 study period compared to the long term average. While these results provide further evidence of deforestation contributing to a downwind drying precipitation trend across different continents and climate regions, five other regions studied showed no significant relation or suggest relative wetting related to deforestation impact. One of this regions is the South America Tropical (SAT) region, the region most well-known for its widespread and intense Amazonian deforestation. The two regions downwind of the SAT region however are highly impacted by SAT deforestation and experience most relative drying in the areas impacted most impacted by deforestation, suggesting strong teleconnecting effects. In the seasonal analysis, only two out of four tropical regions studied show more subregions linking deforestation impact to relative drying in the first wet month compared to the wettest month. While these results provide new insights into the global influence deforestation can have on moisture availability, more research needs to be done into the indirect and feedback effects related to deforestation. Additionally, a more robust way of including other factors influencing precipitation trends like large scale oscillations could further enhance the understanding of this important issue.

1 Introduction

1.1. Background

Human activities directly and significantly influence the global water cycle via land cover changes (Gleeson et al., 2020, Gordon et al., 2005). Societies worldwide are expected to put extra pressure on land use in the coming decades as a response to climate change, adding an extra layer to the indirect impact climate change already has on the hydrological cycle (Chapin III et al., 2008). Humans have currently altered approximately 41% of the Earth's surface, mainly by deforestation in order to expand agricultural land (Sterling et al., 2013). These kind of anthropogenic forcings are now seen as the dominant factor impacting the global water cycle (Gleeson et al., 2020).

1.2. Effects of deforestation on the water cycle

Deforestation has been recognized to have, in general, a bigger impact on moisture flows than other land use changes (Gordon et al., 2005, Sterling et al., 2013). Vegetation and especially trees generally enhance moisture availability via evaporation as leaf area index, root depth and interception losses are higher compared to grasses and crops (Leite-Filho et al., 2019b, Peña-Arancibia et al., 2019, Zhang et al., 2001).

On average, about 40% of continental precipitation has a continental origin (Van Der Ent et al., 2010) and nearly 20% of annual average precipitation on land originates from vegetation-regulated moisture recycling as opposed to moisture recycling from interception, water bodies, soil and melted water. The global and seasonal variability here is large, with some regions receiving almost 50% of their precipitation from vegetation-regulated recycled moisture (Keys et al., 2016). Moisture recycling is defined as the portion of continental precipitation that has evapotranspired over land (van der Ent et al., 2014). Forest also provide crucial climate regulation, carbon storage and habitats for biodiversity richness (Bonan, 2008, Hansen et al., 2013). Still, deforestation continues at a worrying pace with 2.3 million square kilometers forest loss against 0.8 million square kilometers forest gain between 2000 and 2012 (Hansen et al., 2013).

Effects of deforestation are sensitive to location, scale and season (da Silva et al., 2008, Debortoli et al., 2017, Khanna et al., 2017), possibly influencing local, regional and global precipitation differently (Devaraju et al., 2015, Lawrence and Vandecar, 2015, Semazzi and Song, 2001).

1.2.1. Local effects

Local effects occur at the location of deforestation and are dependent on the scale of this deforestation. Devaraju et al. (2015) and Khanna et al. (2017) found that small-scale deforestation in the Amazon rain forest leads to spatial variations in surface roughness and

sensible heat fluxes, which in term leads to thermally triggered mesoscale circulations increasing cloudiness and precipitation over deforested areas. This increase in precipitation has however been linked to a decrease in precipitation on the forested side of the forest-to-nonforest transition zone, when compared to the fully forested situation (da Silva et al., 2008, Knox et al., 2011).

When a certain threshold of deforestation fraction or continued deforested patch size, is exceeded, deforestation leads to a decrease in precipitation (Lawrence and Vandecar, 2015), leading to an overall drier and warmer climate (Knox et al., 2011, Spracklen and Garcia-Carreras, 2015, Spracklen et al., 2012, Zemp et al., 2017). Three decades of Amazonian deforestation have led to a shift in dominant convective regime, from a mostly thermodynamically driven to a dynamically driven regime, leading to drying on the upwind side of the deforested patch due to surface roughness variations suppressing convection (Khanna et al., 2017). Additionally, reductions in precipitation and dry-season intensification could lead to dangerous non-linear self-amplified forest loss (Zemp et al., 2017), amplified by global climate change (Staal et al., 2020).

1.2.2. Including downwind effects

Land cover change and deforestation can also influence non-local and global water dynamics. In other words, changes in land cover in one place (the source area) can be teleconnected to precipitation somewhere else in the region, country or continent (the sink area). The upwind surface and atmosphere that contributes moisture to a specific location's precipitation is called the precipitationshed, while the downwind surface and atmosphere receiving precipitation from a certain location's evaporation can be described as the evaporationshed (Keys et al., 2012, Van Der Ent, 2014).

Local effects like changing river flows (Shiklomanov and Rodda, 2003, Wang-Erlandsson et al., 2018) and altered spatial and temporal patterns of evaporation and transpiration over continents (Gordon et al., 2005, Sterling et al., 2013) thus lead to crucial global knock-on effects including changes in atmospheric moisture feedbacks and teleconnections (Wang-Erlandsson et al., 2018). Local and downwind factors can and do influence a region simultaneously, which can lead to aggravated effects in unfortunate regions where both local and upwind large scale deforestation takes place.

Case studies show the regional effects of these atmospheric teleconnections, focusing for example on the effects of Amazon deforestation (Bagley et al., 2014, Lorenz et al., 2016, Spracklen and Garcia-Carreras, 2015, Spracklen et al., 2012, Werth and Avissar, 2002). Spracklen et al. (2012) found that in more than 60% of the tropics, air that passes extensive vegetation produces at least twice as much rain as air that passes over little vegetation. This shows the importance of large intact patches of forest for downwind precipitation, where precipitation reductions are smaller for more concentrated deforestation leaving larger intact forests compared to small scale spread deforestation (Nobre et al., 2009). The review paper by Lawrence and Vandecar (2015) however suggests the existence of a critical patch size beyond which precipitation is significantly reduced. Looking at actual business-as-usual deforestation in the Amazon, a meta-analysis of regional and global climate model simulation studies found that this will lead to a 8.1 ± 1.4% reduction in Amazon basin precipitation by 2050, exceeding the natural variability (Spracklen and Garcia-Carreras, 2015).

As deforestation leads to a decrease in latent heat flux and a drier atmosphere, this has crucial consequences for regions highly dependent on seasonal precipitation. It has

been found that Amazon deforestation delays the onset, advances the end and shortens the overall length of the rain season (Butt et al., 2011, Costa and Pires, 2010, Leite-Filho et al., 2019a,b). These effects are most apparent at the mesoscale (Debortoli et al., 2017, Leite-Filho et al., 2019b), pointing again to the scale dependency and teleconnected effects of deforestation (Debortoli et al., 2017, Khanna et al., 2017).

1.3. Research objective & relevance

While the used input data, moisture tracking models and resulting relative teleconnections differ (Link et al., 2020), the importance of including moisture recycling and land cover change in global water resource management are evident (Berger et al., 2014, Dirmeyer et al., 2009, Keys et al., 2012, 2016, 2017, 2018, 2019, Link et al., 2020, Sterling et al., 2013, Van Der Ent et al., 2010, Van Der Ent, 2014, Wang-Erlandsson et al., 2018, Wei and Dirmeyer, 2019). Currently, only a few studies have painted a global picture of moisturewise connected areas (Dirmeyer et al., 2009, Link et al., 2020, Sterling et al., 2013, Wei and Dirmeyer, 2019). The aim of this research is thus to explore and where possible quantify the effects of deforestation on annual and seasonal precipitation across the globe. As both the total amount of precipitation as well as the timing are relevant for agricultural practices and ecosystem resilience, both these aspects will be analyzed separately. To conduct the precipitation trend analysis, a novel way of quantifying the global effects of deforestation on local water resources is presented, identifying areas that are potentially most impacted by recent deforestation.

The global evaporationshed database by Link et al. (2020) will form the basis of this research, which links source areas to sink cells after pre-processing into precipitationsheds. Global deforestation will be taken from the Hansen et al. (2013) dataset and compared with recent trends in precipitation compared to longterm averages using MSWEP 1980-2018 precipitation data (Beck et al., 2019). By analyzing a wide variety of different regions, this research aims to find a relation between upwind deforestation and downwind precipitation trends, regionally accounting for other factors that can influence global precipitation trends, like climate zones and multi-year precipitation oscillations.

As the world population continues to grow, so does the pressure on environmental and agricultural systems providing food. Intensive agricultural techniques like double cropping can strengthen local and global food resilience and protect tropical forest that are still intact, however these techniques are highly dependent on rainy season duration (Leite-Filho et al., 2019a,b). Current Amazonian deforestation could push subregions into permanent drier climates, weakening the resilience of the entire region (Malhi et al., 2008). The decline in mean precipitation and redistribution of spatial and temporal precipitation caused by tropical and mid-latitude deforestation also puts agricultural yields in other parts of the world at risk, like in the US, China and India (Lawrence and Vandecar, 2015).

A better understanding of the link between deforestation and downwind precipitation can thus be used to inform regional and international policies on water governance (Keys et al., 2012, 2016, 2017, 2019), enhancing present and future water resilience (Berger et al., 2014, Keys et al., 2019) and providing food security (Keys et al., 2012, 2019, Lawrence and Vandecar, 2015, Leite-Filho et al., 2019a,b, Malhi et al., 2008). Furthermore, this research can complement known benefits of forest conservation and reforestation campaigns (Keys et al., 2012, Leite-Filho et al., 2019a,b) and improve the remote land cover effects in weather and climate models (Wei and Dirmeyer, 2019).

2
Methodology

2.1. Data selection

To compare upwind deforestation and downwind precipitation trends over the 2001-2018 study period, three global datasets are used: an evaporationshed database to link sink and source regions, a deforestation dataset and a precipitation dataset. The temporal and spatial resolution and coverage of the datasets used in this report are summarized in Table 2.1.

2.1.1. Linking sink and source regions

To be able to link sink and source regions with each other, Link et al. (2020) has set up a global evaporationshed database using the Water Accounting Model-2layers (WAM-2layers) moisture tracking model with ERA-Interim input data. Before describing this database and how it will be used in this study, we will first elaborate upon the WAM-2layers model and shortly introduce the ERA-Interim reanalysis data.

WAM-2layers moisture tracking model

The Water Accounting Model-2layers (WAM-2layers) is an Eulerian numerical moisture tracking model that can track tagged moisture flows either forward or backward in time (Van Der Ent, 2014). WAM-2layers has been seen to show consistent results using other tracking methods (Van Der Ent et al., 2013). Input data for this model is taken from reanalysis products, in this case from ERA-Interim (Dee et al., 2011), and includes evaporation, precipitation, wind components in zonal and meridional direction, specific humidity, surface pressure, total column water and total column water vapor. Next to that, it also takes the vertical integral of east- and northward water vapor, cloud liquid water and cloud frozen water flux. The model applies the following water balance equation across the entire grid for each time step:

$$\frac{\partial S_k}{\partial t} + \frac{\partial (S_k u)}{\partial x} + \frac{\partial (S_k v)}{\partial y} = E_k - P_k + \xi_k \pm F_v \tag{2.1}$$

Here, S_k denotes the atmospheric moisture storage in layer k, which can either be the top or bottom layer. t stands for time and u and v represent the wind directions in zonal (x) and meridional (y) directions. The latter two expression left of the = sign thus describe the horizontal moisture flow between grid cells. These three terms have to be in balance with evaporation entering the cell from below (E_k), precipitation leaving the cell (P_k) and the vertical moisture transport entering or leaving the cell layer (F_v). ξ_k is a residual term that appears due to data-assimilation in ERA-Interim and different spatial and temporal resolutions in the calculation steps in WAM-2layers.

Moisture transport in this tracking model is evoked by pressure gradients leading to winds with a certain speed and direction. ERA-Interim additionally includes a convective scheme leading to dispersive moisture transport. This makes it difficult to explicitly calculate the vertical moisture transport F_v, which is taken as the closure term of the water balance. As there also exist a residual term ξ, the water balance is not always fully closed, however these mismatches are mostly negligible (Link et al., 2020, Van Der Ent, 2014). To close this water balance, it is assumed that the top and bottom layer residuals are proportional to the moisture content of these layers. The total WAM-2layers model configuration can be found in Van Der Ent (2014).

ERA-Interim reanalysis data
The ERA-Interim reanalysis dataset (Dee et al., 2011) is developed by the European Centre for Medium-Range Weather Forecasts (ECMWF). Reanalyses combine the strengths of numerical weather models and observations to produce datasets that typically cover the entire Earth and extend over several decades. Reanalysis data is thus spatially complete, however the models and observations used can change over time. Reanalysis datasets like ERA-Interim enable enhanced climate and weather research. More information on ERA-Interim data assimilation, forecast model and observations used can be found in Dee et al. (2011).

ERA-Interim spans from 1979 up to August 2019 and has recently been superseded by the ERA-5 reanalysis. It provides 3-hourly data on surface parameters and 6-hourly upper-air parameters including the troposphere and stratosphere. Details on these output parameters can be found in the ERA-Interim Archive (Berrisford et al., 2009).

Global evaporationshed database
Link et al. (2020) used the WAM-2layers model and ERA-Interim input data to track evaporation forward in time on a global scale. They used 1,5° x 1,5° grid cells from 79,5°N to 79,5°S, excluding oceans, Greenland and Antarctica. The output spans the period of 2001 to 2018, excluding 2000 that was used to spin-up the model. Link et al. (2020) generated five types of output matrices, linking land grid cell, country and basin evaporation to precipitation in all grid cells (land and oceans). Additionally, country and basin evaporation is also linked to country and basin precipitation, respectively. For these output types, one yearly averaged and 12 monthly averaged matrices are produced and available online (Link et al., 2019).

In this study, we want to identify global changes in downwind precipitation on a annual and seasonal scale. For both timescales, we assume changes in linked sink-source areas over the study period to be negligible for the exploratory focus of this research. We will thus use the yearly and monthly averaged moisture transfer matrices, expressed as percentages of the total precipitation in the sink cell. Country and basin borders will be ignored to keep the focus on general upwind-downwind links and processes, so the output matrices linking land grid cell and grid cell will be used for this study.

2.1.2. Landsat deforestation data

From the Landsat 7 database, Hansen et al. (2013) used bands 3, 4, 5 and 7 to compile a global yearly forest extent and change dataset, spanning from 2001 to 2019. This is done by analyzing growing season Enhanced Thematic Mapper Plus (ETM+) scenes using Google

	Spatial		Temporal	
	Resolution	**Coverage**	**Resolution**	**Coverage**
Landsat deforestation (Hansen et al., 2013)	1 arc-second (+/- 30 m at equator)*	Land masses except Greenland and Antarctica	Yearly	2001-2019
MSWEP precipitation (Beck et al., 2019)	0,1° x 0,1°**	Global	Monthly	1980-2018
WAM-2layers evaporation tracking (Link et al., 2020)	1,5° x 1,5°	79,5°S to 79,5°N except Greenland and Antarctica	Yearly and monthly	2001-2018

Table 2.1: Spatial and temporal resolution and coverage for datasets used, where * = downscaled and ** = resampled and downscaled to WAM-2layers 1,5° x 1,5° grid.

Earth Engine (see Supplementary Material of Hansen et al. (2013)). The spatial resolution of the datasets are 1 arc-second per pixel (approximately 30 meters per pixel at the equator).

Forest loss is found using the loss bitmask, where 1 is defined as stand-replacement disturbance (a change from a forest to non-forest state) and 0 as no loss for 2001-2019 (Hansen et al., 2013). This data is used to map the extend of global deforestation and to select sink regions with major deforestation in their respective source regions. The gain bitmask represents forest gain, where 1 is defined as the inverse of forest loss and 0 as no gain for 2001-2012 (Hansen et al., 2013). This mask provides relevant information relating to the scale and extent of global reforestation however only spans part our study period. This data is thus not systematically included in the analysis. Reforested areas that are deforested again in 2001-2019 are labeled as deforested.

2.1.3. MSWEP precipitation data

Global precipitation time series will be collected from the Multi-Source Weighted-Ensemble Precipitation (MSWEP) (Beck et al., 2019). This dataset spans from 1980 to 2018 and reports precipitation every 3 hours on 0.1° grid cells. In this study, monthly 0.1° data will be used, resampled and downscaled to the same 1.5° grid cells as used by WAM-2layers. By combining satellite, gauge and reanalysis data, MSWEP uses the complementary strengths of these methods. Beck et al. (2019) shows for example that CMORPH (satellite data) performs best in moist midlatitude regions while ERA-Interim (reanalysis data) performs best in mid- and high-latitude. MSWEP's method of merging these datasets however also introduces inconsistencies as the overall merging process changes over time and the relative weights per input dataset changes over space.

As this study aims to compare the precipitation changes after upwind deforestation with the yearly and monthly natural variability of precipitation, a dataset specifically focusing on precipitation covering 30+ years is preferred. Next to MSWEP, the Climate Hazards Group InfraRed Precipitation with Stations data (CHIRPS) (Funk et al., 2015) also meets these criteria. CHIRPS however faces the same temporal and spatial inconsistency issues and additionally only spans from 50°S-50°N, thus excludes deforestation hotspots in the high Nothern latitudes (e.g. in Russia, Canada and Alaska). To keep this study as general and exploratory as possible, it is chosen to go forward with MSWEP.

In the latest product, MSWEP V2.6, the datasets used in previous versions (CMORPH, TMPA, 3b42RT, GSMaP-MVK, ERA-Interim and JRA-55) are replaced by ERA5 and IMERG due to their superior performance. More information on V2.6 can be found in Beck (2020).

2.2. Data processing

The aim of this research is to explore and where possible quantify the effects of deforestation on the total amount and timing of global precipitation. In order to answer this question, a novel measure quantifying the downwind effects of deforestation is developed. With this measure, the so-called deforestation impact (I_D) which will be elaborated on below, regions of interest are selected for which a precipitation trend analysis is done. For all regions, the recent yearly precipitation trend relative to the long-term average is compared with the potential deforestation impact, where in general a reverse relation is expected (a drying trend in regions with a high I_D). The South American continent is selected for an additional analysis exploring the relative impacts of local and teleconnected deforestation. For the tropical regions, a seasonal analysis is done comparing the differences in deforestation effect at the beginning of the rainy season, when land evaporation is most limited, and at the peak of the rainy season, when land evaporation is least limited. Data (pre)processing and visualisation is done in Google Earth Engine, Python and QGIS.

2.2.1. Preprocessing evaporationshed to precipitationshed

To be able to select sink regions based on deforestation in the source region, global precipitationshed data is needed to link the sink grid cell to its respective source regions. As Link et al. (2020) provide global evaporationshed data, this needs to be rearranged into precipitationsheds, see Figure 2.1.

Python is used to run through all yearly and monthly averaged sink-source matrices to relate all linked sources to the land sinks. The links are corrected for by a land mask and a land fraction mask, as some cells that are labeled as land cells are actually partly or even mostly sea or ocean, which can lead to misleading contributions. The land mask used is the ERA-Interim land-sea mask, the land fractions mask was provided by Andreas Link as byproduct of the global evaporationshed dataset (see Figures 5.1 and 5.2 in Appendix A). By using these masks to correct for the precipitationshed links, the assumption is made that all parts of the grid cells contribute equally to the moisture flux, highly simplifying reality however still deemed meaningful and accurate enough for the aims of this research.

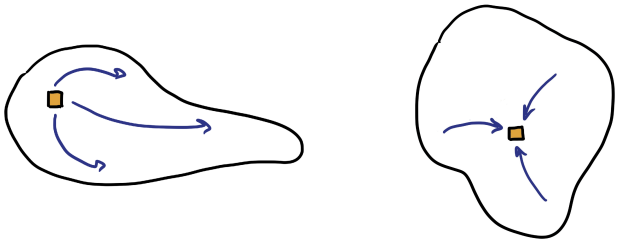

Figure 2.1: Schematisations of an evaporationshed (left) and precipitationshed (right). Yellow square represents the source (sink) cell and blue arrows represent the moisture flows.

2.2.2. Quantifying precipitation impacted by forest cover change

The precipitationsheds computed give an insight into how the sink regions are influenced by water evaporating from the (land based) source areas, however not yet on how deforestation affects these water fluxes. The 'precipitation potentially impacted by deforestation' or

in short 'deforestation impact' (I_D) is thus calculated. This measure assumes that deforested areas do not provide any of the previously evaporated moisture anymore and does not take into account possible feedbacks, making the I_D measure a first order estimate of the influence of the actual recent deforestation on global water supply. The I_D is calculated as the product of the deforestation fraction (F_D) and precipitationshed link percentage (L_P) from the precipitationsheds per 1,5° x 1,5° grid cell, summed together per sink cell (see Figure 2.2):

$$I_{D,x} = \sum_{i=1}^{n} (F_{D,i} * L_{P,i}) \tag{2.2}$$

where n is the number of source cells related to sink cell x.

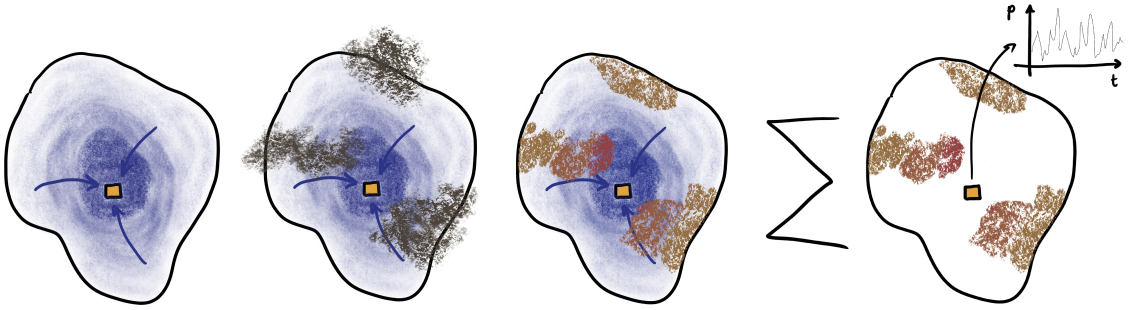

Figure 2.2: Schematisation of a precipitationshed with precipitationshed links (L_P, blue) and deforestation fraction (F_D, brown), together forming the potential deforestation impact (yellow, orange and red) which is summed together for each precipitationshed. Precipitation trend analysis for the sink cell (yellow square) is done afterwards, see Figure 2.3.

As the precipitationshed links are defined as percentages of continental precipitation, I_D is here defined as percentage of continental precipitation as well. Human activities most directly influence the water cycle via land use change, which is most directly visible when I_D is expressed as fraction of continental precipitation. When it is assumed that human activities have the possibility to influence total P_c by for example deforestation, the I_D percentage can be seen as the relative potential influence humans so far have already exerted. In order to see what fraction of actual total precipitation is affected by the measured deforestation, I_D is also converted to percentage of total precipitation using the P_c/P_{total} fraction following from the precipitationshed links and ERA-Interim data (see Figure 5.3 in Appendix B).

The precipitationshed link percentages (L_Ps) are assumed to be approximately steady over the 2001-2018 study period and are represented by the 2001-2018 average links. In drier or wetter years, the overall volume of moisture transfer does change, however the relative contribution of moisture from different areas does not change significantly (according to year-to-year link data, not shown here). This assumption should also be seen relative to the seasonal changes in L_P and I_D, which fluctuate much more in both magnitude and coverage.

The deforestation data provided by Hansen et al. (2013) is accessed using Google Earth Engine (GEE) and downscaled to represent deforestation fractions per 1,5° x 1,5° grid cell.

All land cell precipitationshed link percentages are stored in arrays and are converted to 'bands' in 5 separate GeoTiff datafiles. To be able to use these GeoTiff files in GEE, the files are translated and warped using GDAL to assign a Coordinate Reference System (CRS) and appropriate output bounds. By storing the data as 'bands', which are normally filled with different satellite band data, uploading, processing and downloading the 8684 land cell L_Ps and I_Ds is made more efficient. After multiplying all L_P bands with the downscaled global deforestation data, the datasets are processed again in Python to obtain the sum of the separate bands, which is thus the total I_D per land sink cell.

Next to deforestation, afforestation can also play different roles in the global water cycle. Afforestation is used here for both afforestation, planting of new forests, and reforestation, recovering past forests. The forest cover dataset provided by Hansen et al. (2013) does include global afforestation however only from 2001-2012 and is thus not included formally in the analysis. For completeness and indicative purposes, afforestation impact (I_A) for 2001-2012 is also mapped following the same procedure. This measure should not be interpreted in the same way as I_D however, as newly afforested regions do not provide moisture in the same way as fully grown forests, but can be used to identify regions where afforestation may play a role and to what potential extend.

2.2.3. Downwind precipitation trend analysis

The main part of this research focuses on finding how upwind deforestation influence downwind precipitation trends and whether this possible relation changes seasonally. As this is an explorative research, analysis steps have partly been developed as reaction on found results in earlier steps. In this chapter, we outline the steps taken, define what is meant by precipitation trend and how we aim to account for other factors influencing precipitation trends.

Normalized precipitation cumulative anomalies trend

In order to detect any trends in precipitation in the 2001-2018 study period, the 2001-2018 precipitation ('recent' precipitation) is compared with the 1980-2018 precipitation average ('long term average' precipitation), see Figure 2.3. This is done by computing annual anomalies from the long term average, accumulating these anomalies per year and normalizing these anomalies and cumulative anomalies by the long term average. By normalizing, the anomalies found in areas that were already dry or wet are corrected for this, showing only the relative (accumulated) wetting and drying in 2001-2018, enabling comparison between regions. This measure, representing the recent precipitation trend compared to the long term average, is called the normalized precipitation cumulative anomaly, or $P_{n.cum.an.}$ in short.

Accounting for temporal oscillations and spatial climate variability

Regions with high levels of I_D are selected in order to unravel the relation between deforestation impact and recent precipitation trends. As precipitation trends can be influenced by many different factors, including multi-year precipitation oscillations, proximity to oceans and regional climate, a few steps are taken which aim to single out the possible trend caused by deforestation. Firstly, the regions are not only selected to include as much

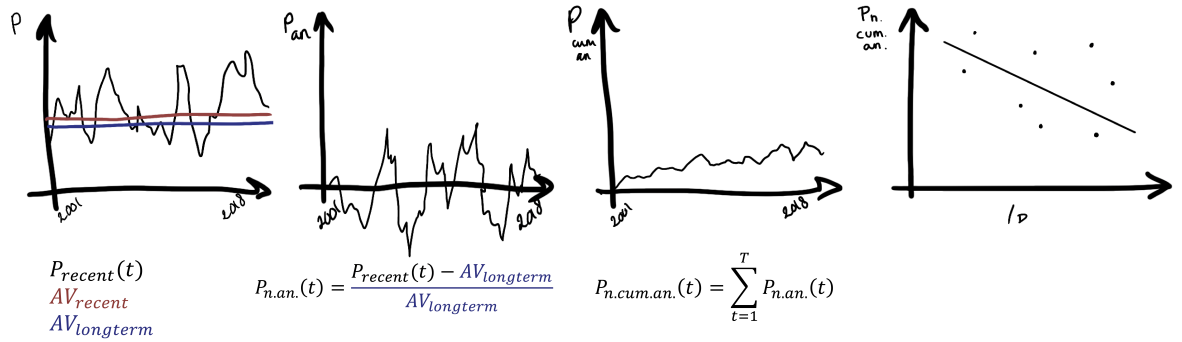

Figure 2.3: Schematisation of precipitation trend analysis for recent (2001-2018) precipitation. By subtracting and normalizing by the long term average and summing these normalized anomalies per year leads to the $P_{n.cum.an.}$ in 2018, which is related with I_D for the regional analysis and in groups of 9 cells in the subregional analysis.

different I_D spread as possible, but also to minimize the influence of climate by delineating regions that are within one climate zone and one (side of a) continent. Climate zones are defined here as the first level classification of Köppen-Geiger, namely Tropical, Dry, Temperate, Cold (or Continental) and Polar. As the I_D - P trend relation is expected to differ for different climates and regions in the world, the aim is to include as diverse range of regions, including different climate zones and continents where possible. A general overview analysis is done per selected region in order to compare the precipitation trend per I_D level from these climate zones and continents with each other.

Secondly, to minimize the influence of spatially changing factors like precipitation oscillations and proximity to oceans, an additional analysis is done using all possible subregions of 9 cells (3 by 3) within the selected regions. The effects of other precipitation influencing factors outside of deforestation are assumed to be negligible within these subregions. For each of these subregions, the normalized cumulative precipitation anomaly is plotted against I_D and the coefficient of the fitted linear line is calculated, see Figure 2.3. Negative coefficients suggest the expected relation between high I_D and a drying P trend, while positive coefficients suggest a wetting trend with higher I_D.

Regional vs. teleconnected effects

In order to explore the relative impact of regional and teleconnected deforestation, the South American continent is selected for an extra calculation. South America is plagued by large spread intense deforestation, concentrated on the borders of the largest tropical rain forest on the planet, making it an interesting case study. In this analysis, the relative contribution of regional deforestation is compared with the relative contribution from SAT deforestation for the total I_D of the SATe and SAD regions.

Analyzing tropical seasonal precipitation

As ecosystems and crops are not only dependent on the total amount of rain but also on the timing and seasonality of precipitation, an additional analysis is done which aims to find out whether the possible relation between I_D and precipitation trends changes seasonally. This analysis is done in selected regions with tropical rainy seasons. The effects

of Amazonian deforestation are found to be more pronounced during the onset and end of the rainy season compared to the peak of the rainy season (Leite-Filho et al., 2019a,b). Amazonian forest have shown to, even during dry periods, sustain evapotranspiration into the atmosphere, compared to deforested areas (Heute et al., 2006). As land evaporation is expected to be most limited at the beginning of the rainy season and least limited during the peak of the rainy season (which seems to be the case for wet Amazonian equatorial sites (Costa et al., 2010)), these two moments are compared to find the difference in deforestation effect and to test this hypothesis. The subregional coefficient analysis is performed for the wettest month (WTM) and first wet month (FWM), which is defined as the first month after the driest month for which the precipitation has risen at least 20% of the difference between the wettest and driest month. The FWM and WTM are defined per subregion.

3
Results

3.1. Mapping potential deforestation impact

Moisture links and actual deforestation data (see Figure 3.1) are used to compute the potential deforestation impact (I_D) per grid cell as defined in Equation 2.2. I_D is defined as a percentage of continental precipitation (P_c), see Figure 3.2. Figure 3.2 highlights areas of which the land based precipitation is most impacted by deforestation, like the Amazon basin, the South-Eastern corner of the US and South-East Asia (Figure 3.2). While the land based precipitationsheds of these areas are all highly impacted by deforestation, these areas have different levels of dependency on continental moisture. Figure 3.3 shows I_D as percentage of total precipitation and corrects for these differences, showing how the actual precipitation a region receives is impacted by deforestation, including oceanic moisture sources. While South-East Asia lights up in Figure 3.2 with up to 50% of P_c potentially impacted by deforestation, Figure 3.3 shows that most cells do not surpass 10% of I_D as percentage of P_{total}. Regions that depend less on oceanic moisture, which are mostly inland areas, light up in Figure 3.3, including West Canada, Siberia, West and Central Africa and most notably South America, around and downwind of recent deforestation (see Figure 3.1).

I_D as percentage of total precipitation will be used in further analysis as it represents the total impact of deforestation, and will from now on be indicated with I_D.

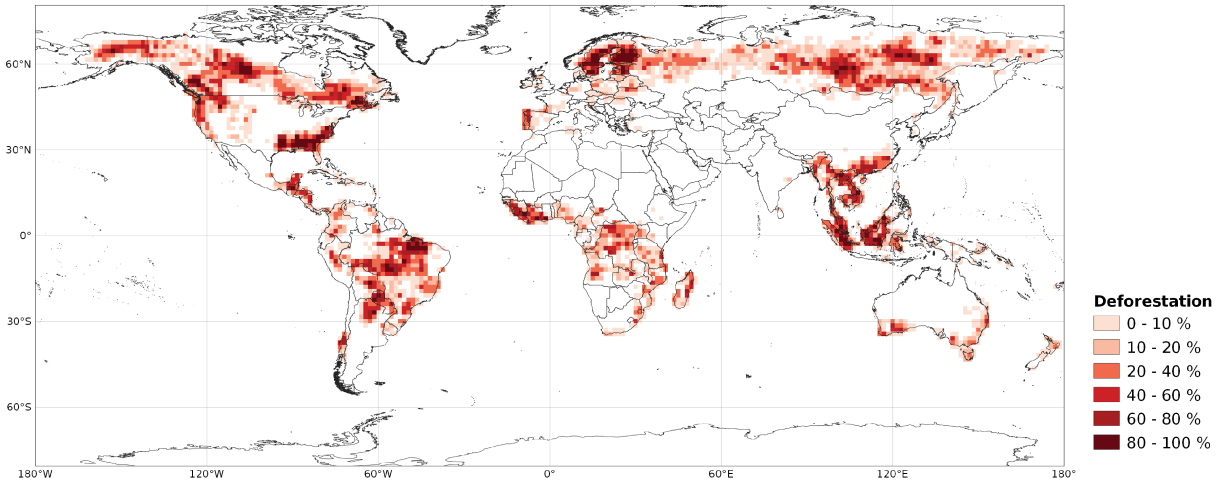

Figure 3.1: Deforestation fraction from 2001-2019 per 1,5° x 1,5° grid cell, after Hansen et al. (2013).

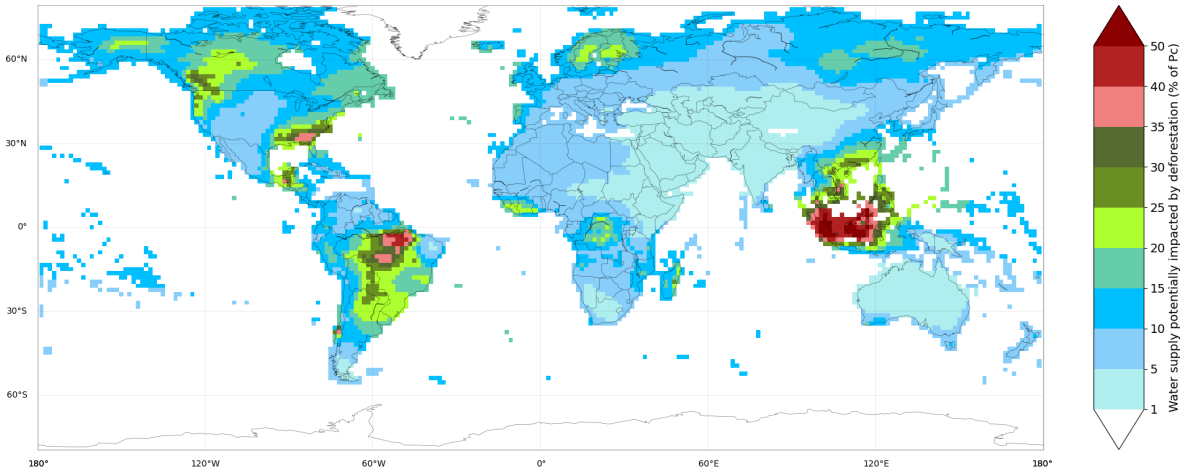

Figure 3.2: Percentage of 2001-2018 averaged precipitation potentially impacted by deforestation as % of continental precipitation.

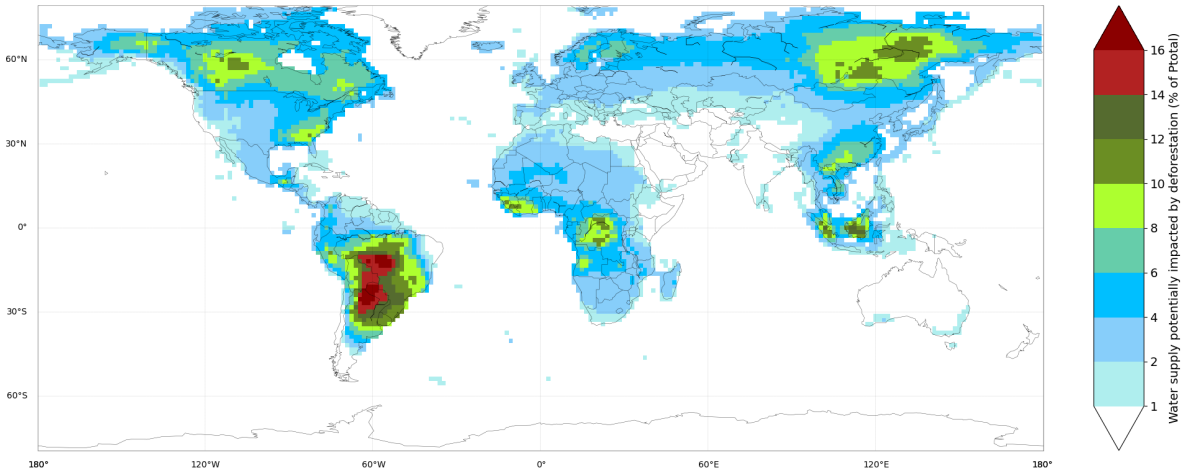

Figure 3.3: Percentage of 2001-2018 averaged precipitation potentially impacted by deforestation as % of total (continental + oceanic) precipitation.

As stated in the Methods, seasonal changes in L_P and I_D (including changes in P_c/P_{total}) are much larger than year to year fluctuations, supporting the assumption of stable L_P links throughout years. Figure 5.4 shows this for the precipitationshed of cell 12974, where seasonally changing wind directions change the direction and coverage of the precipitationshed and the magnitude of the links. Figure 5.5 shows how I_D changes throughout the seasons, showing that the temperate and cold regions fluctuate much more than tropical regions near the equator. This fluctuations are influenced both by the seasonality of these regions, affecting the links between land cells as well as the P_c/P_{total} ratio.

3.2. Deforestation impact on global annual precipitation

The globally selected regions used for all following precipitation trend analyses are shown in Figure 3.4. The regions are named after the (part of the) continent or country they are in (first two letters) and the climate region they are in (last one or two letters), like South America Tropical (SAT), see Table 3.1.

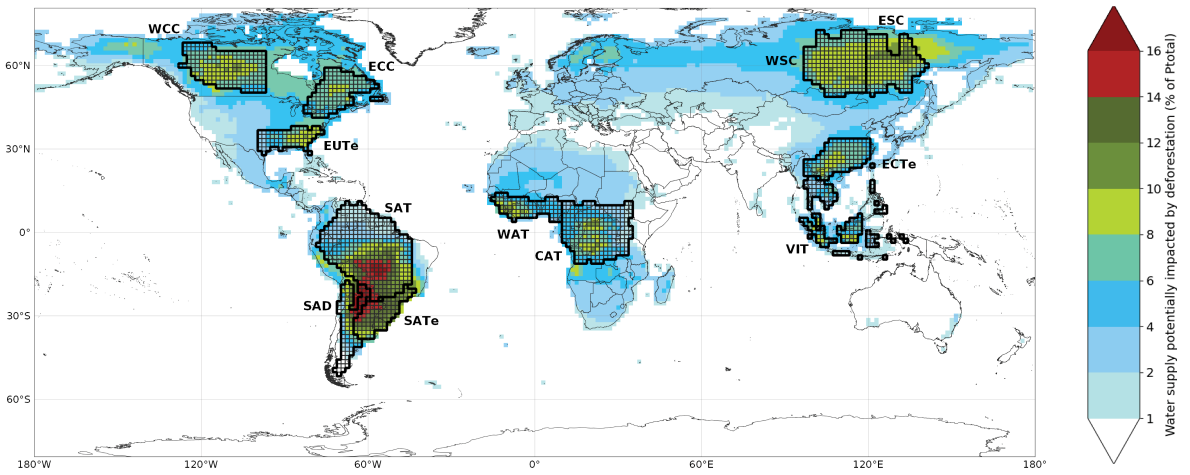

Figure 3.4: Selected regions for precipitation trend analysis. Regions are based on a large spread in I_D and small spread in precipitation oscillations and (first level Köppen-Geiger) climate zones (see Figure 5.8 in Appendix E).

3.2.1. Regional precipitation trend analysis

For all regions, the precipitation trend of each cell is compared to the potential deforestation impact. Figure 3.5 shows the annual development of the normalized precipitation cumulative anomalies and precipitation averaged per I_D level throughout 2001-2018 per region. As expected, the annual precipitation levels vary between different climate zones and regions. Interestingly, some regions see a larger spread between different I_D levels in annual precipitation amount than others. Where the annual precipitation is almost the same for all grid cells in the WCC region, larger differences exist between I_D levels for regions like SAT, VIT and ECTe. While the SAT region cells with highest I_D are drier than others, for VIT and WAT the cells with highest I_D are wetter than others. The recent precipitation trend ($P_{n.cum.an}$) is shown as dotted line in Figure 3.5. Regions like CAT, SATe and SAD show a distinct drying tend which is most pronounced for regions with higher I_D. For other regions, most notably the two regions in Siberia, the normalized precipitation cumulative anomaly shows a wetting trend which is most pronounced for cells with higher I_D. For SAT, EUTe and VIT the averaged normalized precipitation cumulative anomaly fluctuates more around zero, representing little to no drying or wetting compared to the long term average.

In order to better understand the cumulative effects of recent deforestation on the precipitation trend in different grid cells, Figure 3.6 shows the total 2018 $P_{n.cum.an.}$ for all grid cells per region categorized per I_D level. The VIT and CAT regions seem to show a drying trend for cells with a higher I_D above of a certain I_D level, where almost all cells in CAT are drying and almost all VIT cells are getting wetter in relation to the long term average,

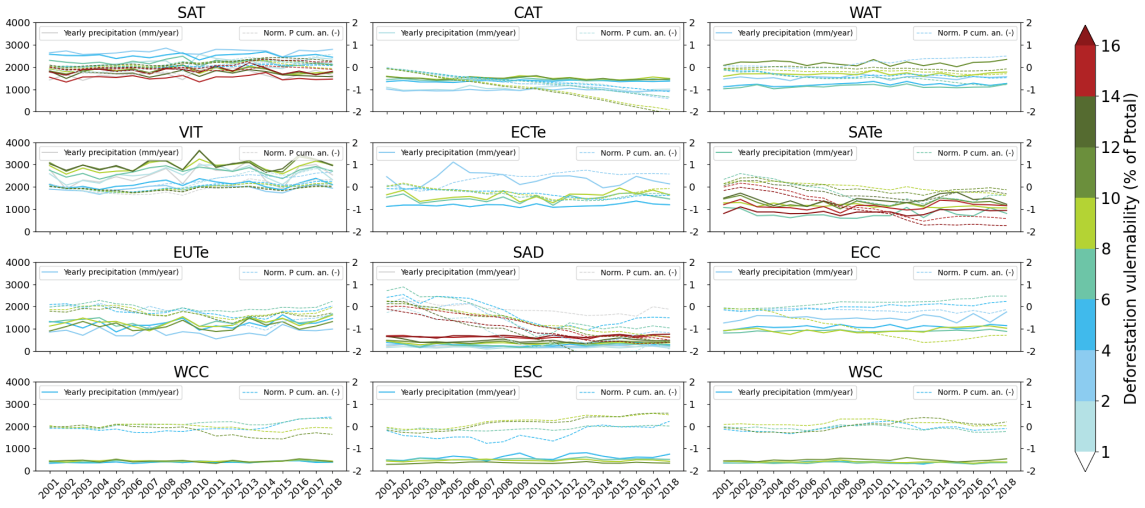

Figure 3.5: Precipitation and normalized P cumulative anomaly development throughout 2001-2018 for all regions, averaged per annual I_D level.

independent of I_D. This suggest that a possible drying effect for higher I_D can be found in both generally wetting as drying regions.

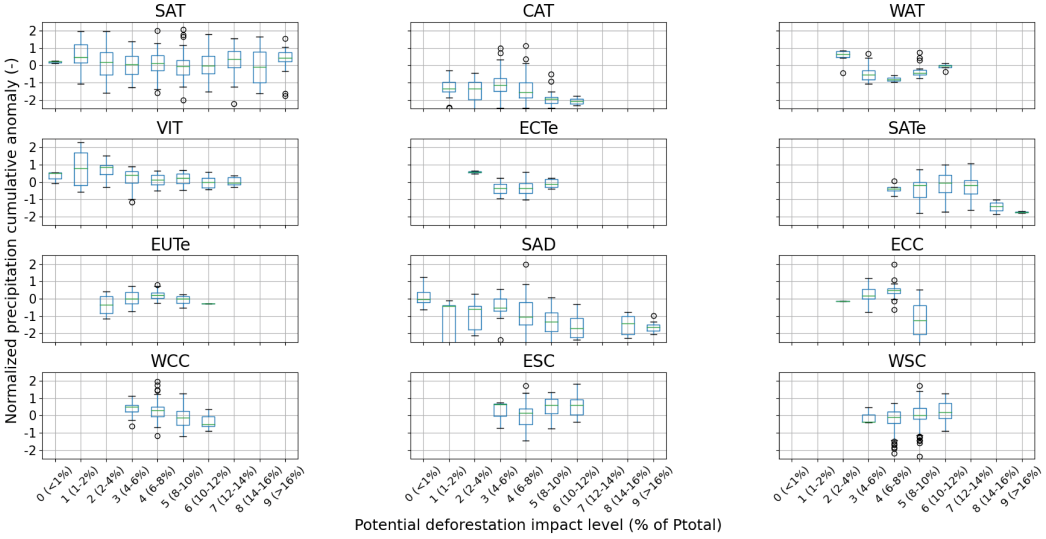

Figure 3.6: Boxplots of normalized yearly precipitation cumulative anomalies per I_D level.

Furthermore, Figure 3.6 shows that only for a few regions the expected relation between I_D and a drying P trend is detected on a regional scale. The largest and most impacted region selected for this study, SAT, shows no clear relation between precipitation trend and I_D as the trend fluctuates around 0 for all deforestation impact levels without a convincing pattern of drying or wetting for subsequent levels. Five regions show a more convincing drying trend with ascending I_D, with at least four subsequent levels getting drier than the previous one (CAT, SATe, SAD, WCC) or a drying trend in five out of six subsequent levels (VIT). The rest of the regions either show a wetting trend with higher I_D for at least four sub-

sequent levels (WSC) or a more fluctuating trend possibly partly due to a smaller number of cells and I_D spread (WAT, ECTe, EUTe, ECC, ESC). While regions within one continent or even within the same climate zone show vastly different trends, unusual relations found for WAT, EUTe and ECC indicate that large differences can also exist between different grid cells within one region.

Region		**Year Co.**	**Year Co. <0**		**FWM Co.**	**FWM Co. <0**		**WTM Co.**	**WTM Co. <0**	
		Sign. fraction of all subregions	All subregions	Sign. subregions	Sign. fraction of all subregions	All subregions	Sign. subregions	Sign. fraction of all subregions	All subregions	Sign. subregions
SAT	South America Tropical	12.1% (31/256)	46.9% (120/256)	48.4% (15/31)	18.8% (48/256)	43.8% (112/256)	35.4% (17/48)	16.8% (43/256)	48.8% (125/256)	53.5% (23/43)
CAT	Central Africa Tropical	28.4% (42/148)	68.2% (101/148)	90.5% (38/42)	32.4% (48/148)	54.7% (81/148)	58.3% (28/48)	33.8% (50/148)	54.1% (80/148)	50.0% (25/50)
WAT	West Africa Tropical	37.0% (10/27)	29.6% (8/27)	10.0% (1/10)	25.9% (7/27)	48.1% (13/27)	42.9% (3/7)	59.3% (16/27)	11.1% (3/27)	6.2% (1/16)
VIT	Vietnam Indonesia Tropical	38.5% (5/13)	84.6% (11/13)	100.0% (5/5)	7.7% (1/13)	15.4% (2/13)	0.0% (0/1)	7.7% (1/13)	69.2% (9/13)	0.0% (0/1)
EUTe	East USA Temperate	29.2% (7/24)	54.2% (13/24)	85.7% (6/7)						
SATe	South America Temperate	37.1% (13/35)	88.6% (31/35)	100.0% (13/13)						
ECTe	East China Temperate	13.8% (8/58)	39.7% (23/58)	12.5% (1/8)						
SAD	South America Dry	21.4% (3/14)	85.7% (12/14)	100.0% (3/3)						
ECC	East Canada Cold	37.9% (22/58)	51.7% (30/58)	68.2% (15/22)						
WCC	West Canada Cold	22.9% (27/118)	65.3% (77/118)	88.9% (24/27)						
ESC	East Siberia Cold	44.6% (37/83)	44.6% (37/83)	37.8% (14/37)						
WSC	West Siberia Cold	14.5% (20/138)	52.2% (72/138)	25.0% (5/20)						

Table 3.1: Subregional analysis relating I_D with $P_{n.cum.an.}$ for subregions of 9 (3 x 3) grid cells, showing percentage of subregions with a coefficients < 0, suggesting a relation between I_D and a drying precipitation trend.

3.2.2. Subregional precipitation trend analysis

As Figure 3.4 shows, cells with a higher I_D are not randomly spread within regions, leaving room for other spatially fluctuating factors like precipitation oscillations and longitudinal and latitudinal location influencing precipitation trends and suggested relations shown in Figure 3.6. This outcome motivated the analysis step presented here, where smaller subregions within the selected regions of 3 by 3 grid cells are used.

Table 3.1 shows per region the percentage of subregions that has a negative coefficient for the fitted linear line between the normalized cumulative precipitation anomaly and I_D, where a negative coefficient suggests a relation between increasing I_D and a drying P trend. Both the percentage of negative coefficients for all subregions as for the significant subregions ($p < 0.05$) are shown here, as well as the percentage of subregions with a significant coefficient. As this is an explorative research and in order to give a more complete picture of the trends found, the not significant results are also presented, however the results discussed in this section concentrate on the subregions with a significant coefficient.

Seven of the analysed regions suggest a relation between I_D and a relative drying P trend in more than 50% of their respective subregions, with five regions (CAT, VIT, SATe, SAD and WCC) showing this relation in over 80% of their subregions. These results are in line with the previous analysis, strengthening the case for a relation between I_D and a drying trend for these five regions while adding EUTe and ECC as two regions where most subregions

suggest a relationship between I_D and a relative drying trend. Both Siberian regions, the WAT region and the ECTe region see more relative wetting in cells with a higher I_D, which is also what Figure 3.4 and Figure 3.7 show us: while there is drying in all these regions, it is lowest in those cells where the potential deforestation impact is highest. The SAT region again does not seem to be influenced by deforestation in its spatially highly fluctuating drying and wetting pattern.

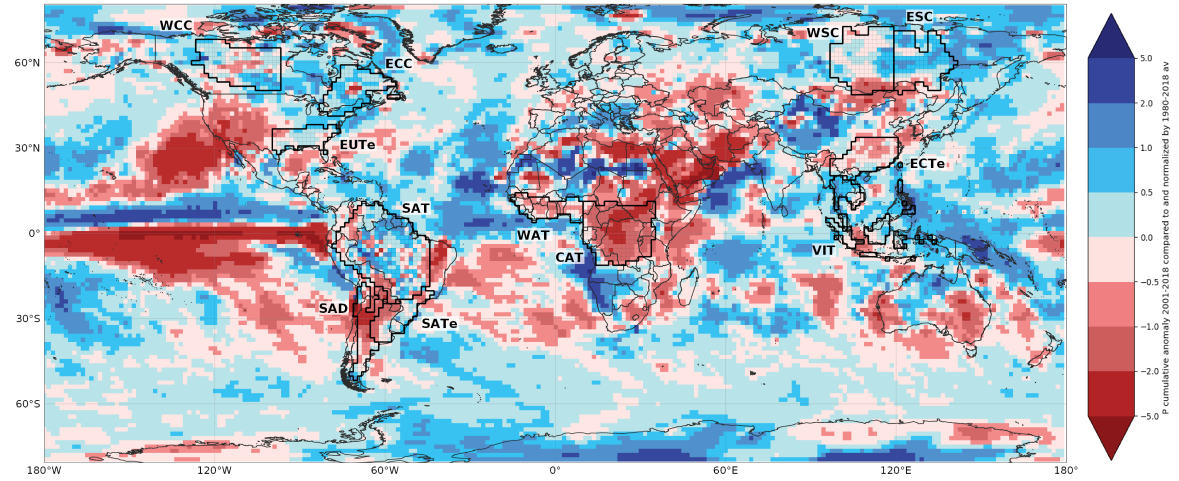

Figure 3.7: Global precipitation cumulative anomalies 2001-2018 compared to and normalized by 1980-2018 average.

Figure 3.8 shows the magnitude and spatial distribution of the subregional coefficients. Some regions stand out with their distinct and abrupt transitions between high contrasting coefficients (WCC, ECC, WSC, ESC and SAT), while the other regions see less extreme coefficients and more fluent transitions. Due to the definition of the coefficients, they are expected to be more extreme when the I_D spread in the subregion is low, which is the case for subregions in Siberia and the Nothern half of SAT. The SAT region has almost as many subregions with a positive as a negative coefficient, contrasting with its neighbouring SATe and SAD regions where a large majority of the subregions suggest a relation between I_D and a relative drying precipitation trend. Figure 3.9 shows the corresponding R^2 values, representing the fraction of variation found in $P_{n.cum.an.}$ explained by I_D. This Figure suggest that I_D in SAT is both linked to drying as well as wetting, while in almost all other regions, R^2 is highest in subregions where I_D is linked to drying. The seven regions with the highest number of subregions suggesting a relation between I_D and a drying trend also show the highest R^2 values for these subregions. The WAT, ECTe and WSC regions show the highest R^2 for subregions that link I_D with wetting, while the ESC region shows strong relations for both subregions linking I_D to wetting and drying.

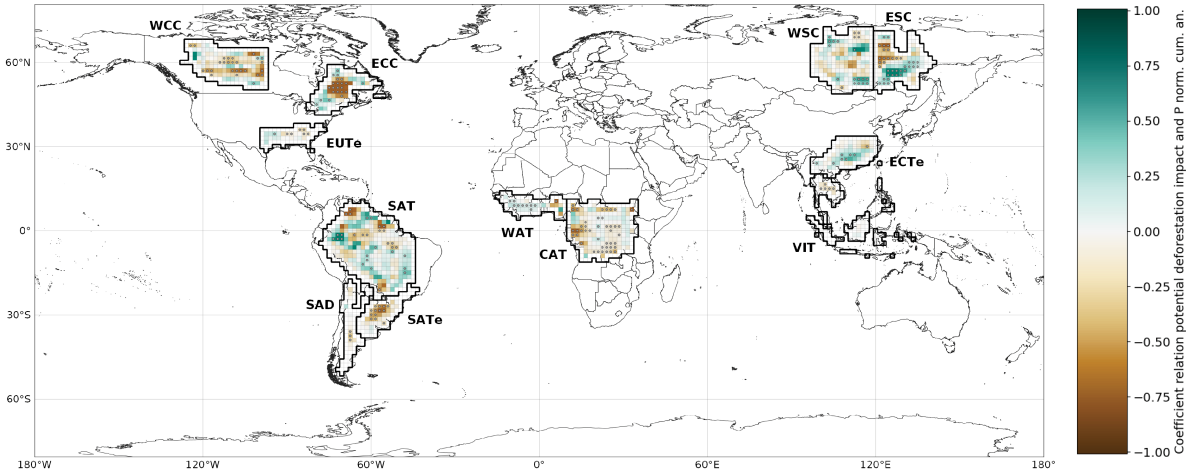

Figure 3.8: Coefficient of subregional relation between annual precipitation trend and changes in I_D, where a negative coefficient suggests a relation between a drying precipitation trend for higher I_D.

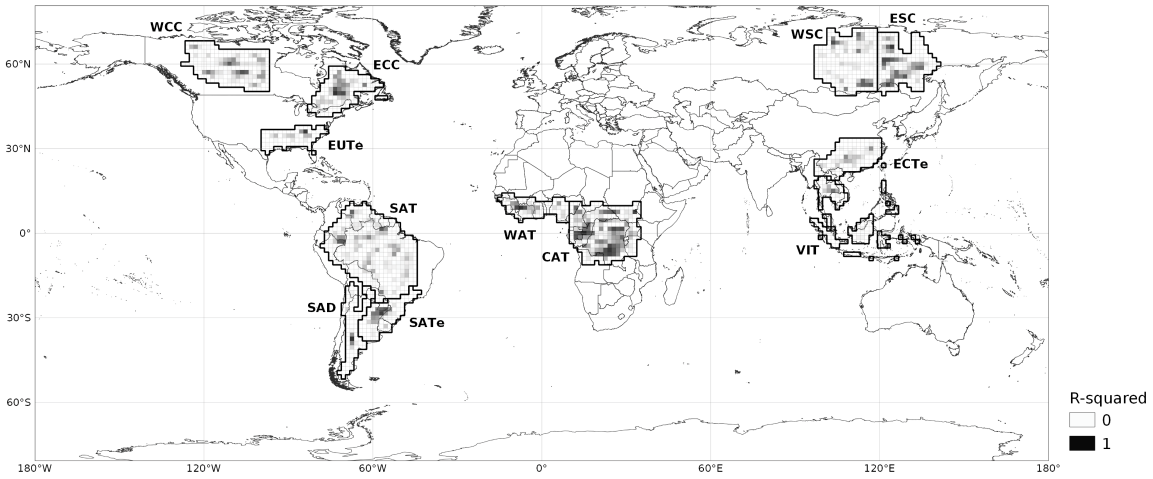

Figure 3.9: R^2 for coefficients of subregional relation between annual precipitation trend and changes in I_D.

3.2.3. Regional vs. teleconnected impact: South America

As seen before, the regional and subregional analysis shows an interesting dynamic for the South American continent, where the SAT region does not show a clear response from deforestation while the other two regions suggest a strong and significant relation between I_D and a drying trend. As stated in the Methods section, the South American continent is selected for an additional step in this analysis aiming to better understand the relative impacts of regional and teleconnected deforestation. Figure 3.10 confirms that while all three regions see high levels of I_D, actual deforestation on the South American continent takes place in the SAT area and even some net afforestation took place from 2001-2012 in the SATe region. It is found that only 8.3% of the total I_D in the SATe region is caused by deforestation within the SATe region borders, while 55.4% is caused by SAT deforestation and 13.7% by SAD deforestation, leaving 22.6% for deforestation elsewhere. For the SAD region, a similar but less strong effect is found: 28.1% of the total I_D is caused by deforesta-

tion within the SAD region while 48.6% is caused by SAT deforestation and 4.7% by SATe deforestation.

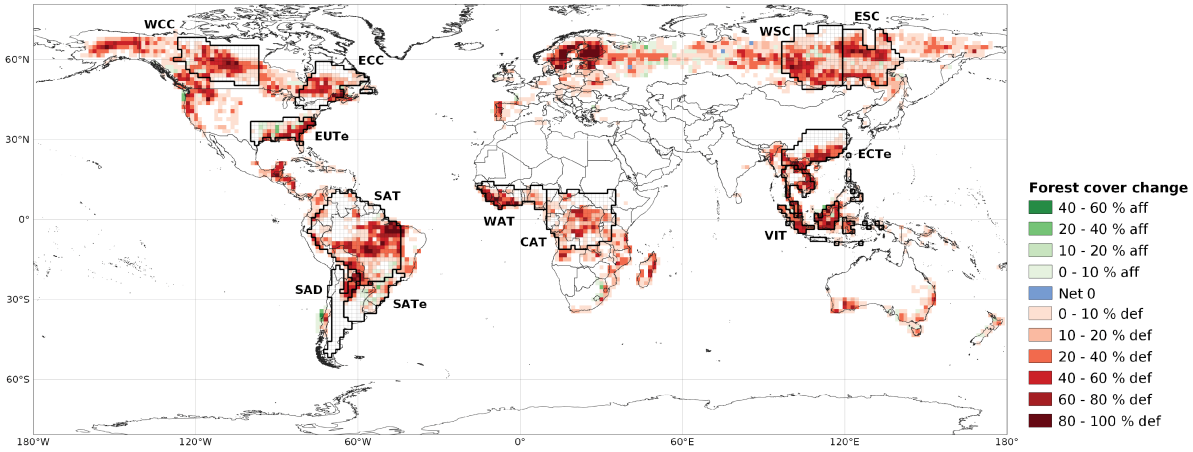

Figure 3.10: Net deforestation (2001-2019) and afforestation (2001-2012) fraction per $1,5°$ x $1,5°$ grid cell, after Hansen et al. (2013). Some deforestation or afforestation might be masked here as net forest cover changes are shown here, while the potential deforestation and afforestation impact only include deforestation and afforestation data respectively. This does not represent the actual net forest cover change as both datasets have different time spans but functions as indication.

3.3. Deforestation impact on tropical seasonal precipitation

Figures 3.11-3.12 show the precipitation, $P_{n.cum.an.}$ and I_D development throughout the year averaged for cells in three different subregions in the four tropical regions. As the seasons change, so do precipitation amounts and trends but also moisture links between grid cells and the P_c/P_{total} fraction, which in turn influences I_D. While the selected regions lie in the same climate zone, large differences between subregions exist in the amount, timing and trend the monthly precipitation averages. The subregions on the equator have a fairly stable $P_{n.cum.an.}$ throughout the year, like subregion SAT 13643, CAT 12495 and VIT 13036, other subregions show larger fluctuations from month to month. Subregions CAT 11528 and WAT 11044 show a similar development, where the first month(s) of the rainy season seem to become drier, while the peak and end of the rainy season see relatively more wetting, suggesting a shifting and intensifying rainy season. Subregions CAT 13701 and WAT 11513 show relative drying just before and just after the peak of the rainy season, with the peak wetting, suggesting a shortening and intensifying rainy season. Mainy regions show large wetting peaks in dry months, which could point to more unpredictable precipitation in months during which there normally is almost no precipitation or a lenghtening of the rainy season, however the relative $P_{n.cum.an.}$ measure by definition results in larger spikes in dry months due to the low average precipitation which is used to normalize.

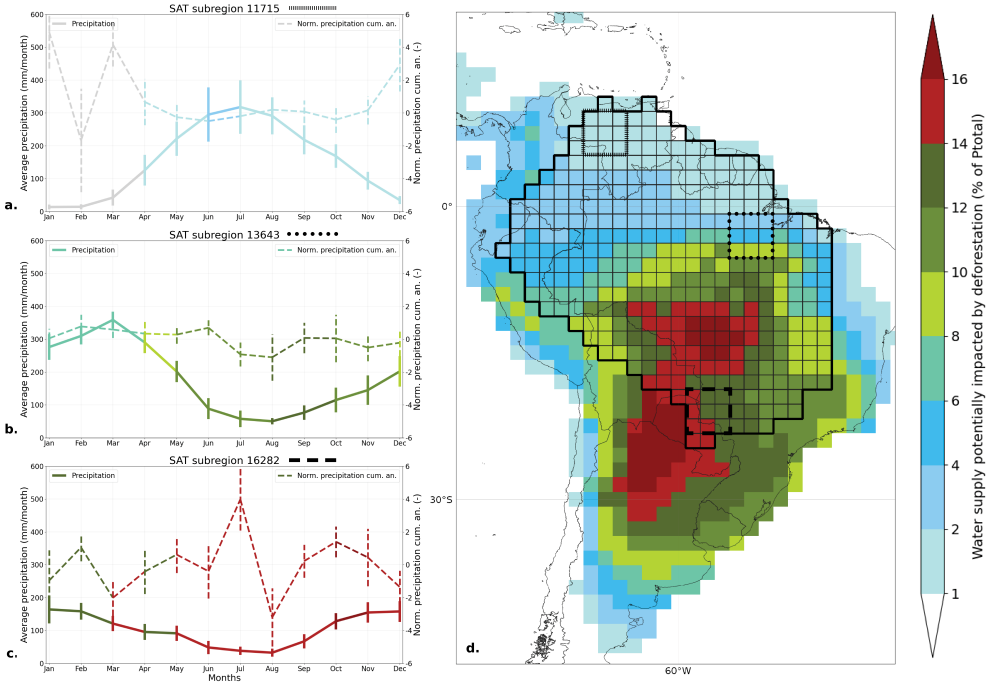

Figure 3.11: SAT seasonal precipitation and $P_{n.cum.an.}$ 2001-2018, averaged for three subregions. Error bars indicate standard deviation.

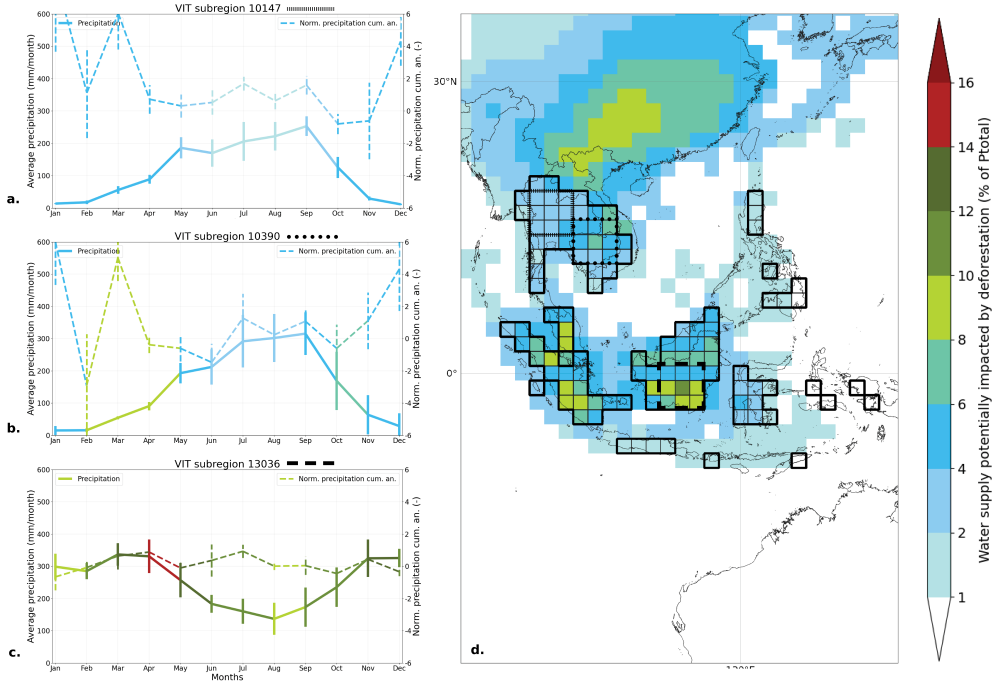

Figure 3.12: VIT seasonal precipitation and $P_{n.cum.an.}$ 2001-2018, averaged for three subregions. Error bars indicate standard deviation.

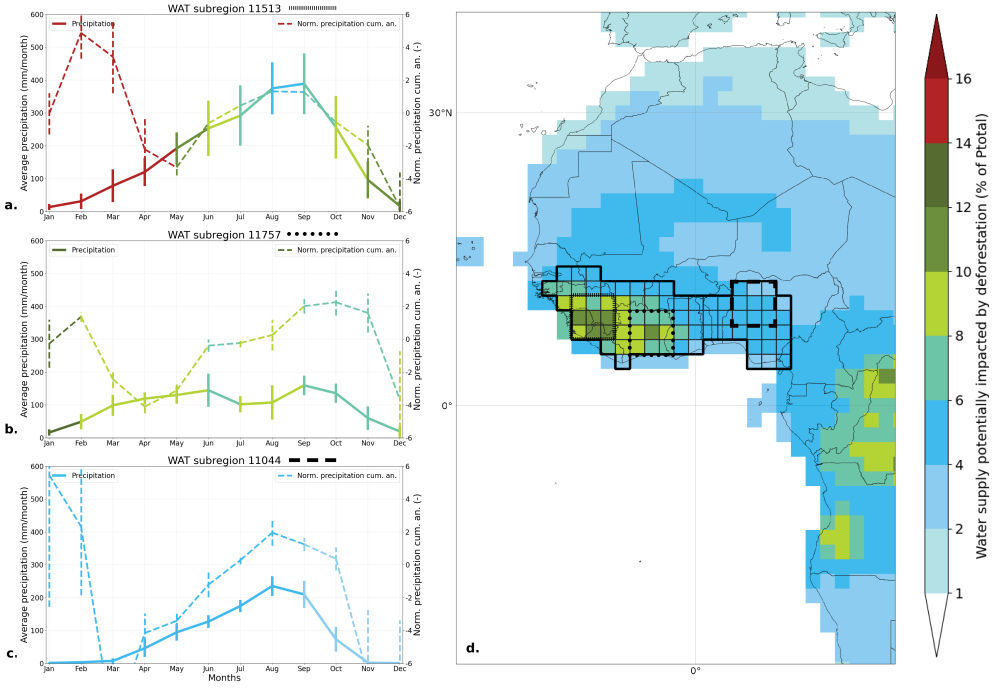

Figure 3.13: WAT seasonal precipitation and $P_{n.cum.an.}$ 2001-2018, averaged for three subregions. Error bars indicate standard deviation.

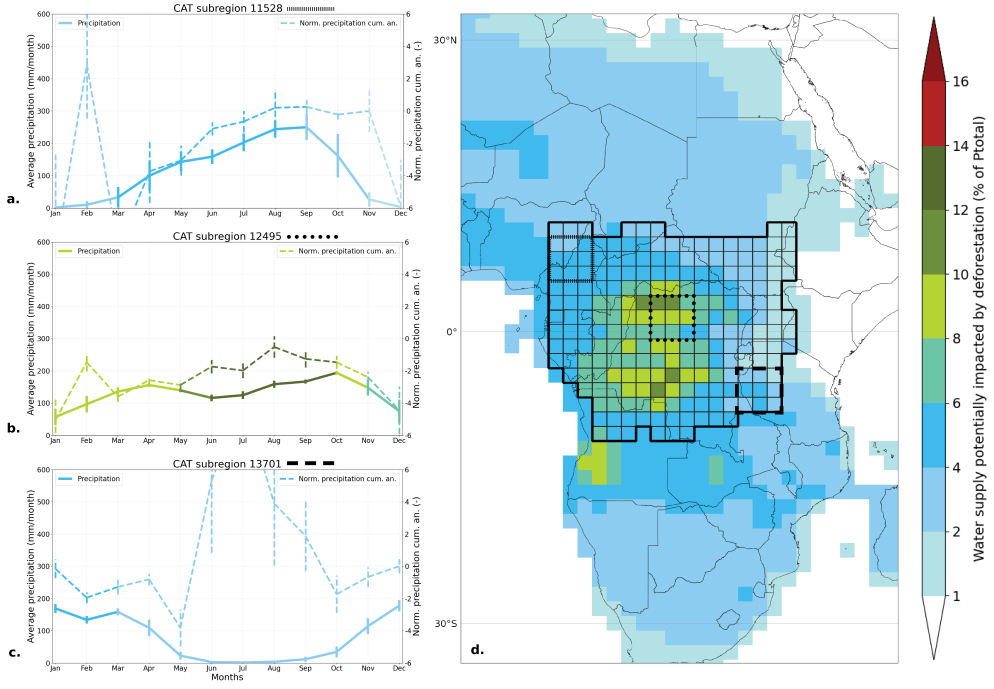

Figure 3.14: CAT seasonal precipitation and $P_{n.cum.an.}$ 2001-2018, averaged for three subregions. Error bars indicate standard deviation.

Table 3.1 shows that in the WAT and CAT regions, more subregions points towards a relation between I_D and a drying precipitation trend in the first wet month (FWM) compared to the wettest month (WTM), confirming the expected pattern, while the SAT region shows the opposite signal. No clear result is found for the VIT region as only one subregion shows a significant coefficient, however a similar pattern is found as for the SAT region when all subregions are included.

Furthermore, the VIT and CAT region both have lower percentages for the FWM and WTM compared to the average, suggesting other months or seasons in which I_D has a stronger relationship with a drying trend. Figure 3.15 show that the Northern SAT and mainland VIT subregions fluctuate highly between the FWM and WTM, showing both more drying in the WTM locally (however not significant for VIT). Interestingly, almost half of the WAT subregions suggest a relation between I_D and a drying precipitation trend in the FWM, with the significant suggesting this relation subregions all in the Eastern half of the region. The CAT subregions show little difference in coefficient pattern between the FWM and WTM, with only a slight increase in extreme coefficients in the FWM and a Northward shift of significant coefficient subregions.

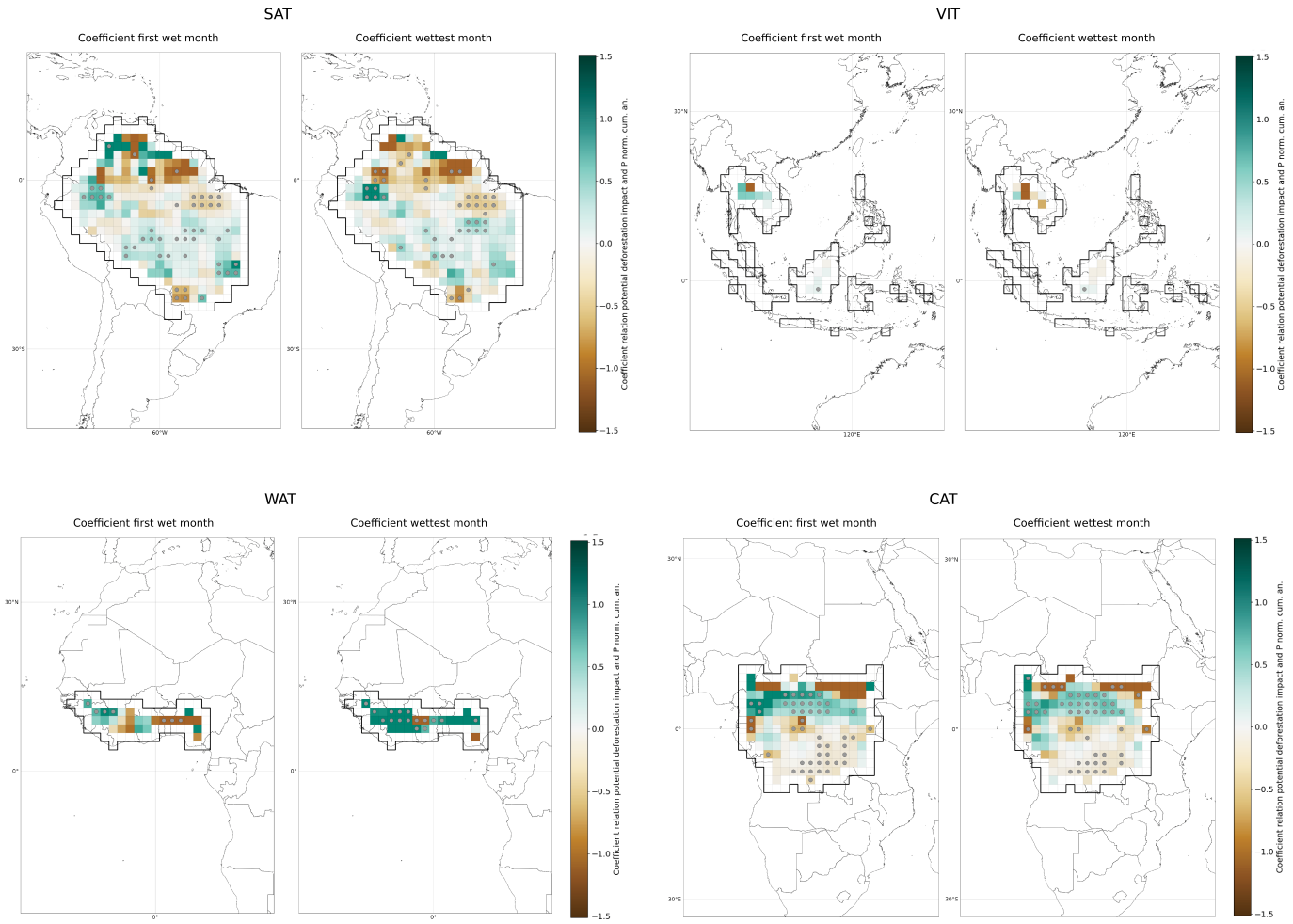

Figure 3.15: Coefficient of tropical subregional relation between first wet month and wettest month precipitation trend and changes in I_D, where a negative coefficient suggests a relation between a drying precipitation trend for higher I_D. Driest, first wet and wettest months per subregion are shown in Figure 5.9 in Appendix F.

4
Discussion

4.1. Limitations of potential deforestation impact

Indirect and feedback effects of deforestation

The potential deforestation impact (I_D) measure does not take into account indirect effects and possible feedback mechanisms of deforestation, while these could be significant (Alkama and Cescatti, 2016, Aragão et al., 2008, Nobre et al., 2009, Runyan et al., 2012, Staal et al., 2020). As forests are able to evaporate more water and interact with their environment in order to sustain their own living conditions (Runyan et al., 2012), deforestation can trigger forest diebacks, fires and droughts. This is of particular concern as both human induced and natural deforestation and forest management currently often involve fire, which may become more difficult to handle in drier conditions. Previous research in the Amazon demonstrates that fires and droughts enhance each other, leading to increasing risks of dangerous reinforcing feedbacks (Aragão et al., 2008, Staal et al., 2020). Deforestation could even lead to an irreversible state where forest vegetation cannot recover, putting both reforestation and forest conservation in a new light (Runyan et al., 2012). Deforestation is also linked to large scale impacts on for example El Niño-Southern Oscillation (ENSO) activity leading to reduced rainfall over the Amazon (Nobre et al., 2009) and rising global mean and maximum temperatures (Alkama and Cescatti, 2016), contributing indirectly to enhanced forest loss. Not taking these mechanisms into account implies that the results presented in this study are probably underestimations and possibly also spatially distortions of the actual impact of recent deforestation on moisture flows.

Replacing land use cover

Another possibly significant factor that is not taken into account is the land use cover replacing the deforested areas. In the calculation of I_D, it is assumed that deforested areas do not contribute any moisture to the sink cell anymore, however this simplification does not take into account the varying moisture generating capacities of other types of land use cover. This factor is of extra importance when deforested land is replaced by irrigated agricultural lands, possibly replacing part of the moisture supply lost by deforestation. Gordon et al. (2005) found that while most areas have a net decrease in vapor flows after deforestation including irrigation, some locations within the ECTe and VIT region also show a major net increases in water vapor due to irrigation. Local irrigational practices could be part of the explanation of the strong relation between I_D and a wetting precipitation trend in the ECTe region and are worth looking into more systematically.

4.2. Deforestation impact on annual precipitation

Uncertain influence of deforestation

Next to uncertain effects from other factors on precipitation trends, deforestation itself also can have different kinds of impacts on precipitation trends depending on the scale, pattern and location of deforestation. Deforestation can locally lead to an increase in precipitation for example at the deforested side of a forest-to-nonforest zone (Knox et al., 2011) or regionally due to increased surface roughness and sensible heat fluxes (Devaraju et al., 2015, Khanna et al., 2017), up to a certain deforestation fraction or continued deforested patch size threshold (Lawrence and Vandecar, 2015). The SAT region is overall getting wetter recently when compared to the long term (see Figure 3.5 and 3.7), however when comparing actual deforestation in Figure 3.1 with the coefficients in Figure 3.8, one finds subregions linking I_D with relative drying mostly in highly deforested areas, while relative wetting is related to I_D on the downwind (South-West) edge of the intensely deforested SAT area. This is in line with recent findings of Khanna et al. (2017), who state that three decades of Amazonian deforestation has shifted the precipitation regime from thermodynamically to dynamically driven, suppressing convection upwind and enhancing convection in the downwind section of the deforested region. These different deforestation effects can possibly explain why the SAT region, well known for its major deforestation, has a small majority of subregions that suggest a relation between I_D and a wetting precipitation trend. While this result differs from the expected relation and from the suggested link in other (neighbouring) regions, Lawrence and Vandecar (2015) finds that evidence for a trend in total annual rainfall in the Amazon region related to deforestation is indeed mixed.

These opposing signals can also possibly explain the low R^2 values found compared to other regions. For the seven regions where a majority of subregions suggest a link between I_D and a drying precipitation trend, high R^2 values are overrepresented at subregions where this relation is detected, suggesting that a large part of the precipitation trend found is related to I_D, however correlation does not mean causation. As no other factors are taken into account to attribute changes in $P_{n.cum.an.}$ to, this measure should only be interpreted relative to other regions. It should also be noted that the subregional analysis assumes a linear relationship between I_D and $P_{n.cum.an.}$ which is probably not the case and a possible reason for low R^2 values in most subregions.

Uncertain influence of other factors

The trends suggested in the 12 different regions analyzed vary quite a bit, where there potential deforestation impact per region and the suggested relations with the precipitation trend do not seem to have a strong link with the local climate zone. The cold regions in Siberia suggest very different relations than the cold regions in Canada, which amongst themselves also show different deforestation impact patterns. For many regions, it remains difficult to draw conclusions on the relation between deforestation impact and precipitation trend, expressed as I_D and $P_{n.cum.an.}$. Even with both a regional as well as subregional analysis, it remains uncertain whether other factors influencing precipitation trends play a role, either by masking deforestation effects or by distorting the possible relation between I_D and a drying precipitation trend. The subregional analysis provides more detailed and robust results however the rubregions used are still quite large as a result of the coarse precipitationshed data, leaving room for other factors to skew the found relation. Dividing the

region in subregions and leaving not significant coefficients out also significantly lowered the available data points per region. Further research preferably uses higher resolution data in order to more specifically isolate deforestation impacts on precipitation trends and increase the number of data points.

Separating regional and downwind deforestation impact
The found deforestation impact of SAT in the downwind SATe and SAD regions confirms the suggestion emerging from other analyses and earlier research. Debortoli et al. (2017) pointed in this direction by looking into different scales of influence for Amazonian deforestation, however did not link this explicitly to teleconnected influences. Spracklen et al. (2012) shows the importance of large intact forests for downwind precipitation, which this result seems to confirm for the South American continent. While the SAT region is much larger than both downwind regions, this result acknowledges that regions with little to no deforestation hundreds of kilometers can be substantially impacted by deforestation. That more than 80% of the SATe and SAD subregions suggest a relative drying trend related to I_D emphasizes the relevance of taking teleconnected effects into account. Further research should however be done into the factors that construct this effect like deforestation intensity, location and proximity and in other regions and continents around the world.

4.3. Deforestation impact on tropical rainy seasons

Expected and found results
While previous research found significant relations between deforestation and a lengthening of the dry season, a delay in onset and an advanced demise of the rainy season (Butt et al., 2011, Costa and Pires, 2010, Leite-Filho et al., 2019a,b), the current analysis found only for two out of four tropical regions (WAT and CAT) a stronger relationship between deforestation and a drying trend in the first wet month compared to the wettest month. Even though many different definitions exist of onset and demise, previous research agrees on changes in onset of around 0.5 days and demise of 1.34 days per year due to prior Amazonian deforestation (Butt et al., 2011, Leite-Filho et al., 2019a,b). While fairly significant over a period of 18 years, with the current research set up it appears to be difficult to find the extra influence deforestation is thought to have at the beginning of the rainy season compared to the wettest period (Leite-Filho et al., 2019b). As stated earlier, the subregional analysis is not ideal as it still encompasses quite large areas, assumes a linear relationship and limits the number of datapoints, which make interpreting the results more difficult.

Spatially varying precipitation drivers
The SAT region, a region where I_D seems more linked to a drying trend during the wettest month, is very dependent on large scale precipitation oscillations such as ENSO activity and the Atlantic north-south sea surface temperature (SST) gradient for its wet and dry season precipitation, respectively (Malhi et al., 2008). A stronger SST gradient is found to result in a delay in onset and advance in demise (Marengo et al., 2001), however the SST influences are not the same over the South American continent. As an effect, total annual precipitation for regions close to the equator are mostly affected by the length of the rainy season, while it is more affected by the precipitation rate in regions affected by the South

Atlantic Convergence Zone (SACZ) (Liebmann et al., 2007). Additionally, Costa et al. (2010) found that evapotranspiration of the wet equatorial forests is driven only by abiotic factors while it is also influenced by biotically controlled factors, like water stress in vegetation, for seasonally dry forest. Such factors influence the SAT subregions' precipitation and evapotranspiration in different ways, making comparison over the whole region complex.

Spatially varying rainy season

The current set up of this analysis compared the first wet month with the wettest month, however does not take into account the fact that for three out of four tropical regions, namely CAT, WAT and VIT, there is mostly not one well defined rain season peak (see Figure 5.9). As the first wet month is defined as a fraction of the absolute peak, this could form a bias towards later months for regions where the second rainy season peak is larger. The definition of the first wet month is thus not very well suited for these tropical regions and should be improved in further research.

5
Conclusion

This research provides a new approach to quantify first order influence actual deforestation has on global moisture flows and precipitation trends. Comparing potential deforestation impact (I_D) with annual precipitation trends ($P_{n.cum.an.}$) suggests a relation between high I_D and a drying precipitation trend in more than half of the subregions for seven regions (CAT, VIT, SATe, EUTe, SAD, ECC and WCC), however the effect of other factors and the exact effect of local and teleconnected deforestation on precipitation trends remains uncertain. While the SAT region does not show a relation between I_D and a drying precipitation trend, the two downwind regions SATe and SAD both show this relation in more than 80% of their subregions. 55.4% of the calculated potential deforestation impact of the SATe region is caused by deforestation in the SAT region as opposed to 8.3% from deforestation in the region itself. For the SAD region, 48.6% of calculated I_D is caused by deforestation in SAT, 28.1% by deforestation within the SAD region boundaries. Only two out of four tropical regions, WAT and CAT, show a stronger relation between I_D and a drying precipitation trend for the first wet month compared to the wettest month, while previous research suggests the strongest deforestation influence on Amazonian drying for the beginning and end of the rainy season compared to the peak (Leite-Filho et al., 2019a).

The feedback between deforestation and enhanced droughts is expected to become stronger with ongoing climate change (Staal et al., 2020). Deforestation already exacerbates warming (Alkama and Cescatti, 2016) possibly leading to irreversible conditions in which forest vegetation cannot recover (Runyan et al., 2012). Lawrence and Vandecar (2015) summarize that deforestation has shown to reduce agricultural productivity locally, regionally and globally by limiting average moisture resources, enhancing temperature extremes and shortening seasonal precipitation periods, contrary to the intentions of agricultural expansion. Malhi et al. (2008) concludes that protecting global forests from unbridled deforestation needs effective policy and governance structures in place and a strong political will at the local, national and international level. The teleconnected effects of deforestation on the amount and timing of precipitation as suggested in this and earlier studies emphasizes the importance of this last and perhaps most complex level, as deforestation at one side of the globe can significantly impact moisture availability at the other side. Including the effects of deforestation climate feedback mechanisms, large scale precipitation oscillations and smaller regions with a higher resolution should be considered in future research in order to enhance the understanding of deforestation effects on precipitation trends.

Appendix

A. Land fraction and land-sea mask

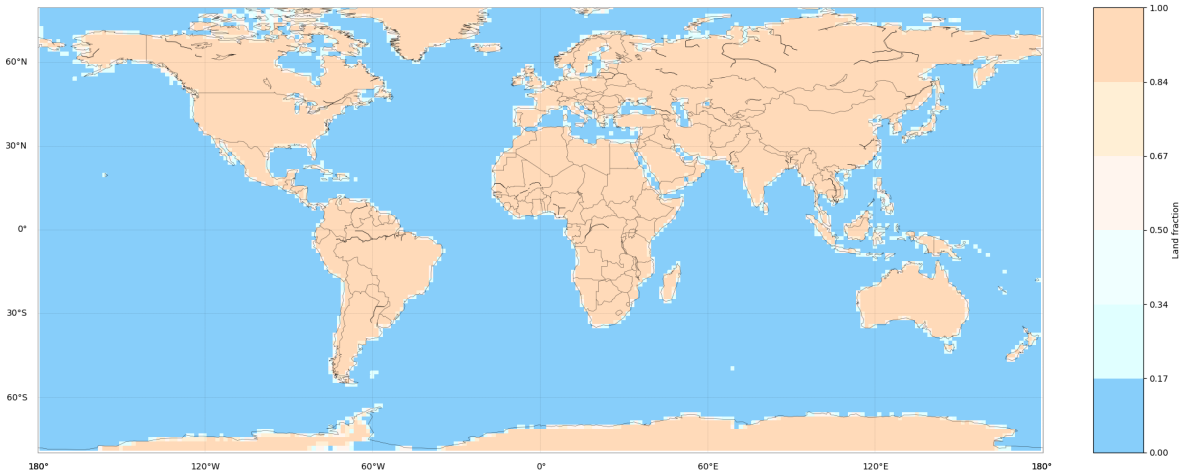

Figure 5.1: Land fractions by Andreas Link

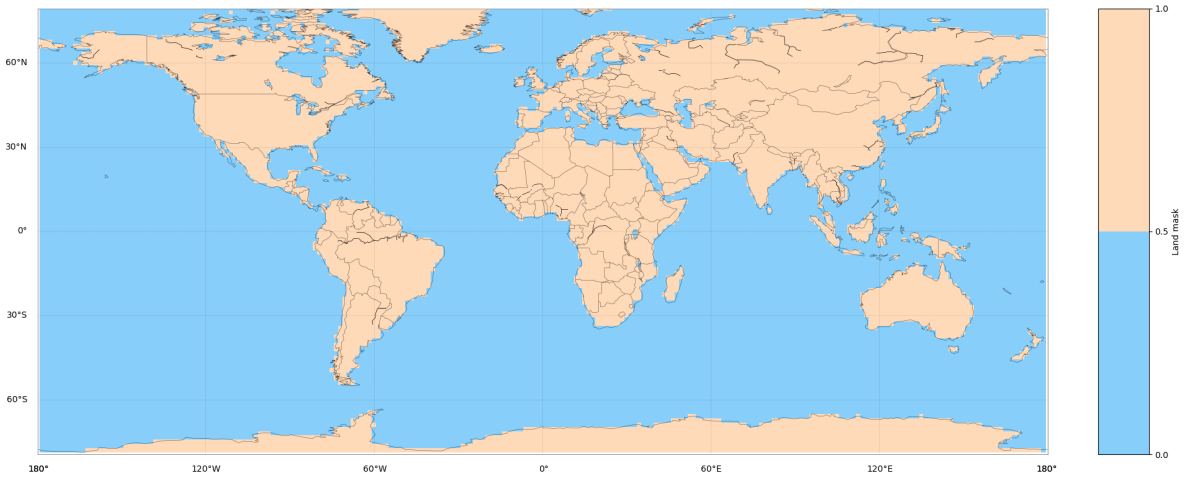

Figure 5.2: Land-sea mask ERA-Interim

B. P_c/P_{total}

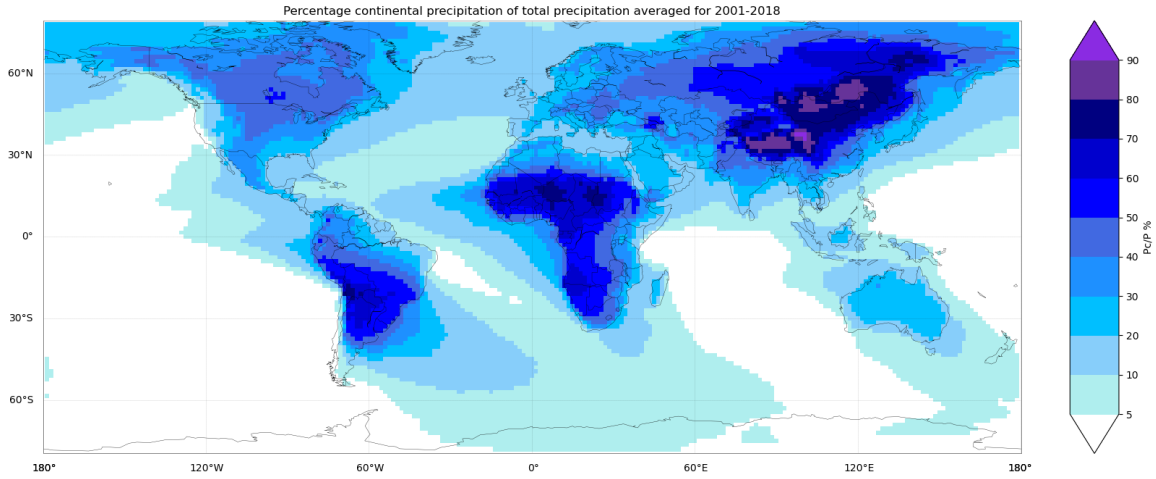

Figure 5.3: Percentage continental precipitation of total precipitation averaged for 2001-2018 from WAM2-layers input data, showing where the continental recycling of moisture is high and which areas are potentially vulnerable to land use changes like deforestation in their respective source areas.

C. Seasonality precipitationsheds and I_D

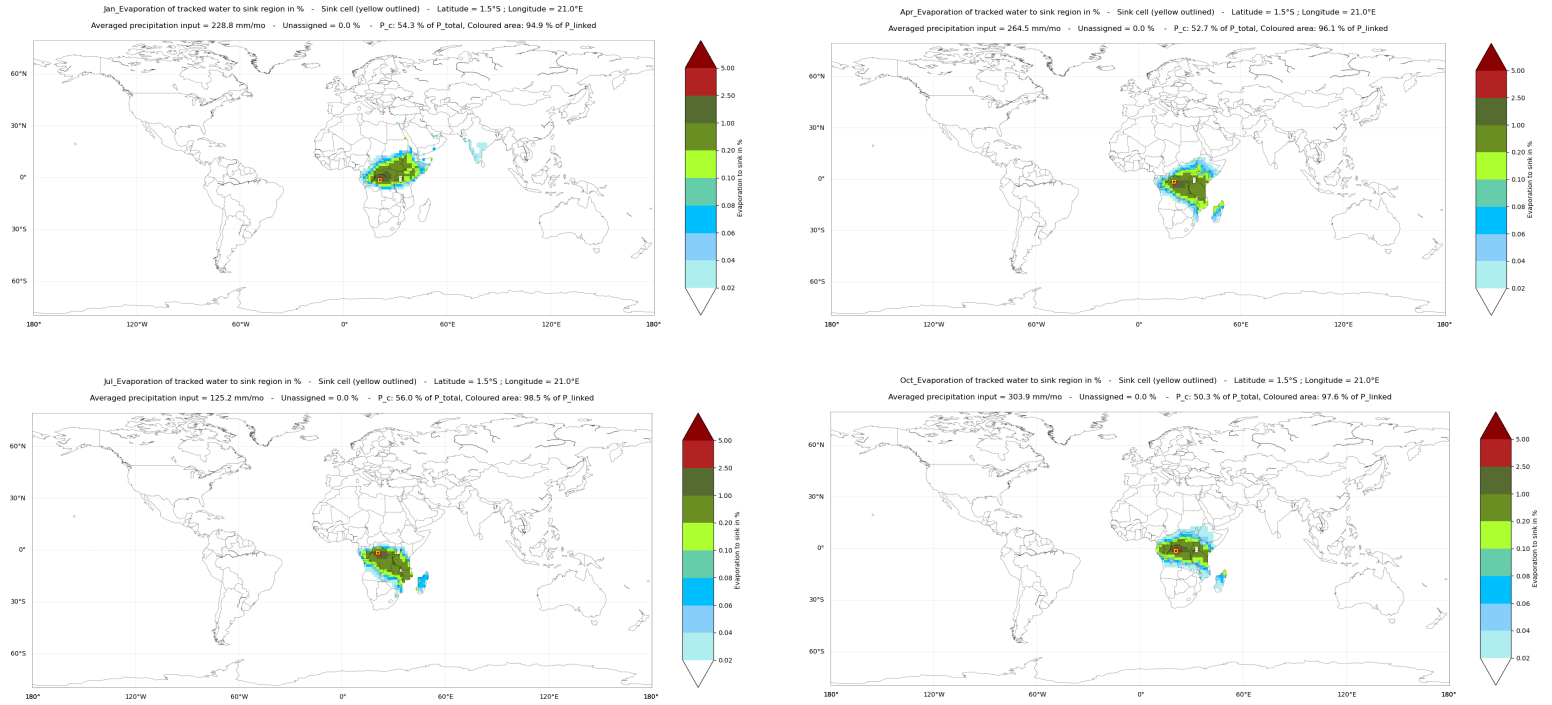

Figure 5.4: Precipitationsheds cell 12974 for January, April, July and October averaged over 2001-2018.

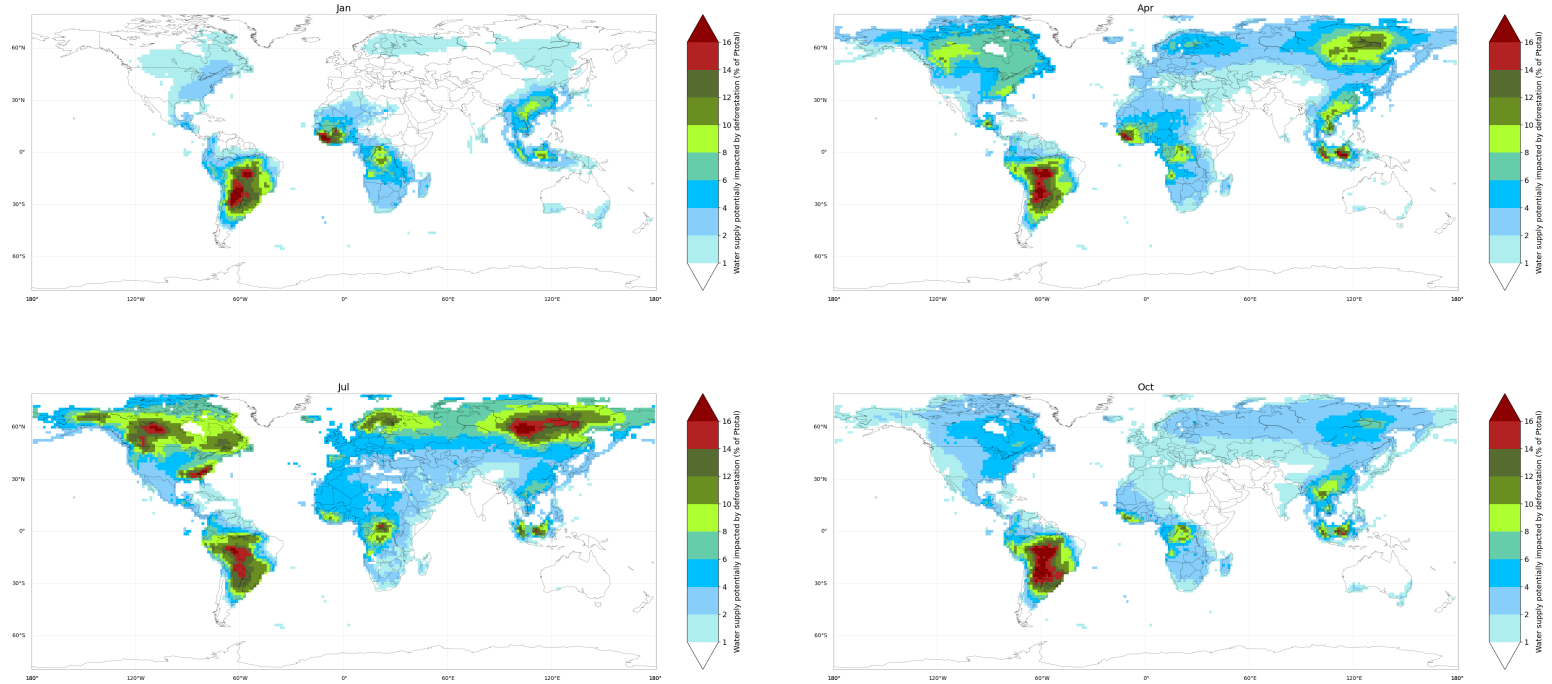

Figure 5.5: Potential deforestation impact (I_D) for January, April, July and October averaged over 2001-2018.

D. Potential afforestation impact

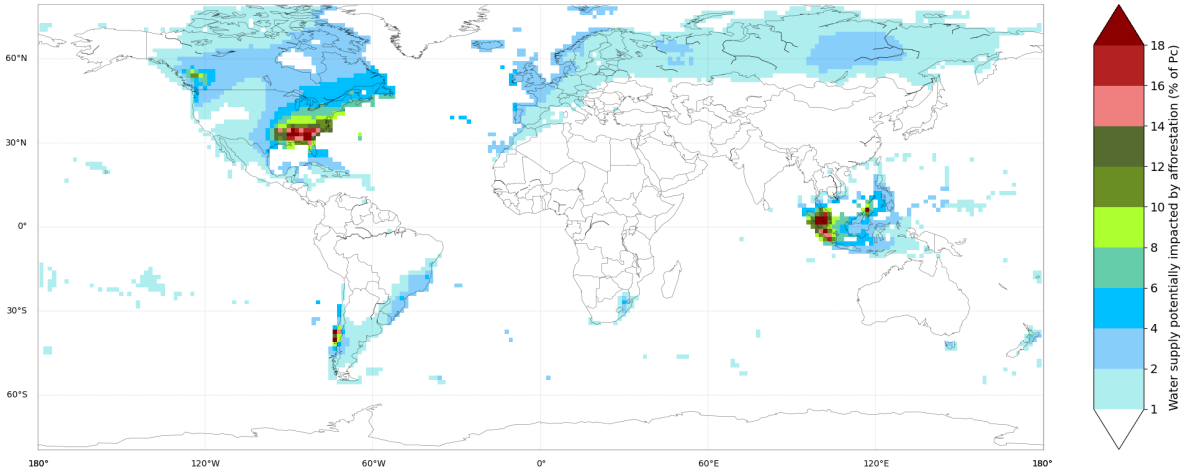

Figure 5.6: Percentage of 2001-2012 averaged precipitation potentially impacted by afforestation as % of continental precipitation. The regions most impacted are the East of US, Canada, parts of South America and Indonesia.

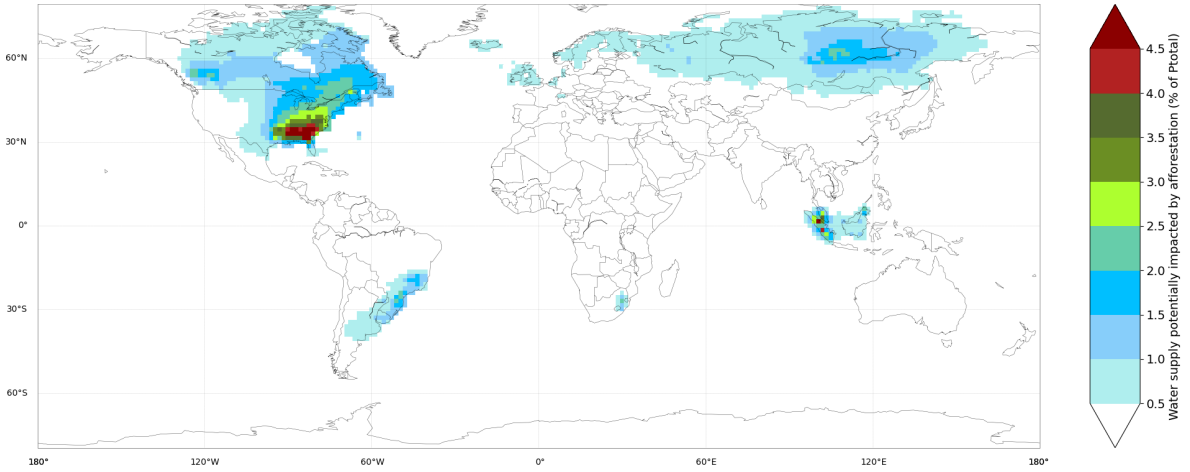

Figure 5.7: Percentage of 2001-2012 averaged precipitation potentially impacted by afforestation as % of total precipitation. The regions most impacted are the East of US, Canada, parts of South America, Russia and Indonesia.

E. Selected regions and Köppen-Geiger climate zones

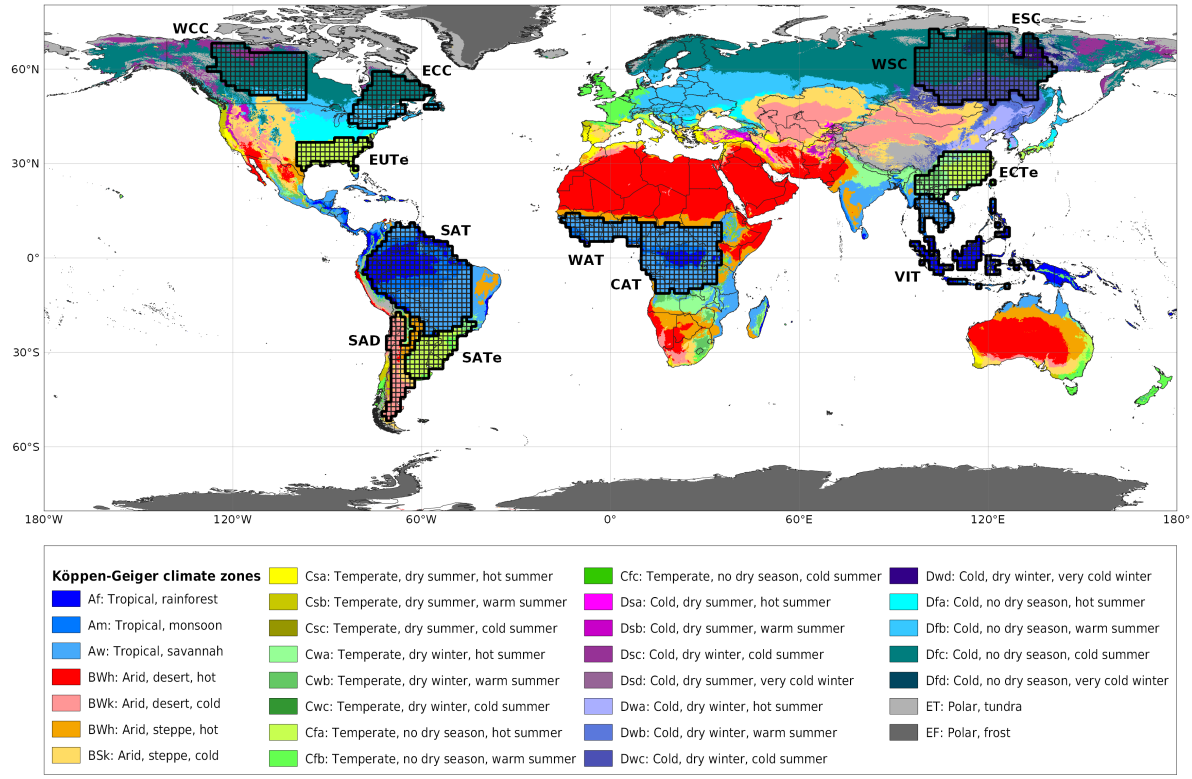

Figure 5.8: Selected regions for precipitation trend analysis. Regions are based on a large spread in I_D (see Figure 3.4) and small spread in first level Köppen-Geiger climate zones.

F. Tropical regions driest, first wet and wettest month

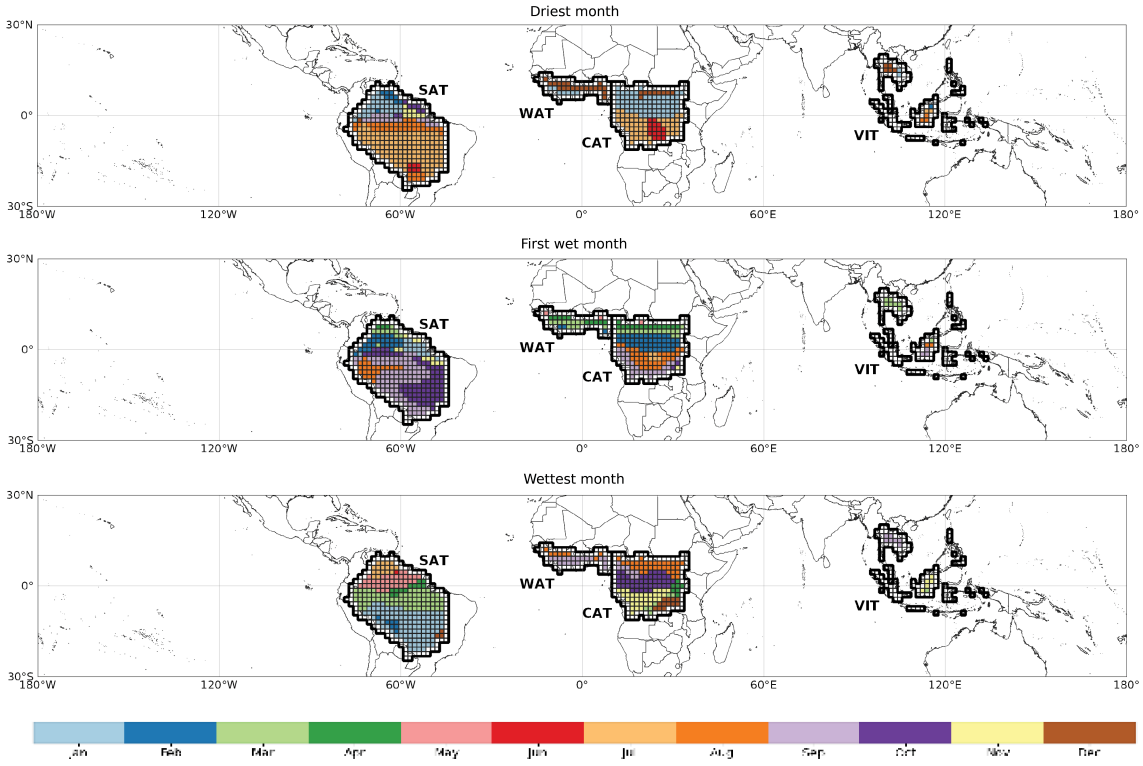

Figure 5.9: Driest, first wet and wettest month for the tropical regions. Showing a similar onset pattern in South America dependent on longitude as well as latitude as earlier studies (Leite-Filho et al., 2019a).

Bibliography

Ramdane Alkama and Alessandro Cescatti. Climate change: Biophysical climate impacts of recent changes in global forest cover. *Science*, 351(6273):600–604, 2016. ISSN 10959203. doi: 10.1126/science.aac8083.

Luiz Eduardo O.C. Aragão, Yadvinder Malhi, Nicolas Barbier, Andre Lima, Yosio Shimabukuro, Liana Anderson, and Sassan Saatchi. Interactions between rainfall, deforestation and fires during recent years in the Brazilian Amazonia. *Philosophical Transactions of the Royal Society B: Biological Sciences*, 363(1498):1779–1785, 2008. ISSN 09628452. doi: 10.1098/rstb.2007.0026.

Justin E. Bagley, Ankur R. Desai, Keith J. Harding, Peter K. Snyder, and Jonathan A. Foley. Drought and deforestation: Has land cover change influenced recent precipitation extremes in the Amazon? *Journal of Climate*, 27(1):345–361, 2014. ISSN 08948755. doi: 10.1175/JCLI-D-12-00369.1.

Hylke Beck. MSWEP Version 2.6 documentation. pages 1–5, 2020.

Hylke E. Beck, Eric F. Wood, Ming Pan, Colby K. Fisher, Diego G. Miralles, Albert I.J.M. Van Dijk, Tim R. McVicar, and Robert F. Adler. MSWep v2 Global 3-hourly 0.1° precipitation: Methodology and quantitative assessment. *Bulletin of the American Meteorological Society*, 100(3):473–500, 2019. ISSN 00030007. doi: 10.1175/BAMS-D-17-0138.1.

Markus Berger, Ruud Van Der Ent, Stephanie Eisner, Vanessa Bach, and Matthias Finkbeiner. Water accounting and vulnerability evaluation (WAVE): Considering atmospheric evaporation recycling and the risk of freshwater depletion in water footprinting. *Environmental Science and Technology*, 48(8):4521–4528, 2014. ISSN 15205851. doi: 10.1021/es404994t.

Paul Berrisford, D. Dee, K. Fielding, M. Fuentes, P. Kallberg, S. Kobayashi, and S. Uppala. The ERA-Interim Archive. 2009. URL http://www.ecmwf.int/publications/library/do/references/list/782009{%}5Cnhttp://centaur.reading.ac.uk/1997/.

Gordon B Bonan. Forests and Climate Change : Climate Benefits of Forests. (June):1444–1449, 2008.

Nathalie Butt, Paula Afonso De Oliveira, and Marcos Heil Costa. Evidence that deforestation affects the onset of the rainy season in Rondonia, Brazil. *Journal of Geophysical Research Atmospheres*, 116(11):2–9, 2011. ISSN 01480227. doi: 10.1029/2010JD015174.

F Stuart Chapin III, James T Randerson, A David McGuire, Jonathan A Foley, and Christopher B Field. Changing feedbacks in the climate – biosphere system In a nutshell :. *Front. Ecol. Environ.*, 6(6):313–320, 2008. doi: 10.1890/080005.

Marcos H. Costa, Márcia C. Biajoli, Luciana Sanches, Ana C.M. Malhado, Lucy R. Hutyra, Humberto R. Da Rocha, Renata G. Aguiar, and Alessandro C. De Araújo. Atmospheric versus vegetation controls of Amazonian tropical rain forest evapotranspiration: Are the wet and seasonally dry rain forests any different? *Journal of Geophysical Research: Biogeosciences*, 115(4):1–9, 2010. ISSN 01480227. doi: 10.1029/2009JG001179.

Marcos Heil Costa and Gabrielle Ferreira Pires. Effects of Amazon and Central Brazil deforestation scenarios on the duration of the dry season in the arc of deforestation, 2010. ISSN 08998418.

Renato Ramos da Silva, David Werth, and Roni Avissar. Regional impacts of future land-cover changes on the Amazon basin wet-season climate. *Journal of Climate*, 21(6):1153–1170, 2008. ISSN 08948755. doi: 10.1175/2007JCLI1304.1.

Nathan S. Debortoli, Vincent Dubreuil, Marina Hirota, Saulo Filho Rodrigues, Diego P. Lindoso, and Jean Nabucet. Detecting deforestation impacts in Southern Amazonia rainfall using rain gauges, 2017.

D. P. Dee, S. M. Uppala, A. J. Simmons, P. Berrisford, P. Poli, S. Kobayashi, U. Andrae, M. A. Balmaseda, G. Balsamo, P. Bauer, P. Bechtold, A. C.M. Beljaars, L. van de Berg, J. Bidlot, N. Bormann, C. Delsol, R. Dragani, M. Fuentes, A. J. Geer, L. Haimberger, S. B. Healy, H. Hersbach, E. V. Hólm, L. Isaksen, P. Kållberg, M. Köhler, M. Matricardi, A. P. Mcnally, B. M. Monge-Sanz, J. J. Morcrette, B. K. Park, C. Peubey, P. de Rosnay, C. Tavolato, J. N. Thépaut, and F. Vitart. The ERA-Interim reanalysis: Configuration and performance of the data assimilation system. *Quarterly Journal of the Royal Meteorological Society*, 137(656):553–597, 2011. ISSN 00359009. doi: 10.1002/qj.828.

N. Devaraju, Govindasamy Bala, and Angshuman Modak. Effects of large-scale deforestation on precipitation in the monsoon regions: Remote versus local effects. *Proceedings of the National Academy of Sciences of the United States of America*, 112(11):3257–3262, 2015. ISSN 10916490. doi: 10.1073/pnas.1423439112.

Paul A. Dirmeyer, Kaye L. Brubaker, and Timothy DelSole. Import and export of atmospheric water vapor between nations. *Journal of Hydrology*, 365(1-2):11–22, 2009. ISSN 00221694. doi: 10.1016/j.jhydrol.2008.11.016. URL http://dx.doi.org/10.1016/j.jhydrol.2008.11.016.

Chris Funk, Pete Peterson, Martin Landsfeld, Diego Pedreros, James Verdin, Shraddhanand Shukla, Gregory Husak, James Rowland, Laura Harrison, Andrew Hoell, and Joel Michaelsen. The climate hazards infrared precipitation with stations - A new environmental record for monitoring extremes. *Scientific Data*, 2:1–21, 2015. ISSN 20524463. doi: 10.1038/sdata.2015.66.

Tom Gleeson, Lan Wang-Erlandsson, Miina Porkka, Samuel C. Zipper, Fernando Jaramillo, Dieter Gerten, Ingo Fetzer, Sarah E. Cornell, Luigi Piemontese, Line J. Gordon, Johan Rockström, Taikan Oki, Murugesu Sivapalan, Yoshihide Wada, Kate A. Brauman, Martina Flörke, Marc F.P. Bierkens, Bernhard Lehner, Patrick Keys, Matti Kummu, Thorsten Wagener, Simon Dadson, Tara J. Troy, Will Steffen, Malin Falkenmark, and James S. Famiglietti. Illuminating water cycle modifications and Earth system resilience in the Anthropocene. *Water Resources Research*, 56(4):1–24, 2020. ISSN 19447973. doi: 10.1029/2019WR024957. URL https://doi.org/10.1029/2019WR024957@10.1002/(ISSN)1944-9208.GRANDCHAL1.

Line J. Gordon, Will Steffen, Bror F. Jönsson, Carl Folke, Malin Falkenmark, and Åse Johannessen. Human modification of global water vapor flows from the land surface. *Proceedings of the National Academy of Sciences of the United States of America*, 102(21):7612–7617, 2005. ISSN 00278424. doi: 10.1073/pnas.0500208102.

M. C. Hansen, P.V. Potapov, R. Moore, M. Hancher, S. A. Turubanova, A. Tyukavina, D. Thau, S. V. Stehman, S. J. Goetz, T. R. Loveland, A. Kommareddy, A. Egorov, L. Chini, C. O. Justice, and J. R. G. Townshend. Global Forest Change. URL https://earthenginepartners.appspot.com/science-2013-global-forest/download{_}v1.7.html.

M. C. Hansen, P.V. Potapov, R. Moore, M. Hancher, S. A. Turubanova, A. Tyukavina, D. Thau, S. V. Stehman, S. J. Goetz, T. R. Loveland, A. Kommareddy, A. Egorov, L. Chini, C. O. Justice, and J. R. G. Townshend. High-Resolution Global Maps of. 850(November):850–854, 2013. doi: 10.1126/science.1244693.

R.A. Heute, K. Didan, E.S. Yosio, P. Ratana, S.R. Saleska, L.R. Hutyra, W. Yang, R.R. Nemani, and R. Myneni. Amazon rainforests green-up with sunlight in dry season, 2006.

P. W. Keys, R. J. Van Der Ent, L. J. Gordon, H. Hoff, R. Nikoli, and H. H.G. Savenije. Analyzing precipitationsheds to understand the vulnerability of rainfall dependent regions. *Biogeosciences*, 9(2): 733–746, 2012. ISSN 17264170. doi: 10.5194/bg-9-733-2012.

Patrick W. Keys, Lan Wang-Erlandsson, and Line J. Gordon. Revealing Invisible Water: Moisture Recycling as an Ecosystem Service. *PLoS One*, pages 165–166, 2016. doi: 10.4121/uuid.

Patrick W. Keys, Lan Wang-Erlandsson, Line J. Gordon, Victor Galaz, and Jonas Ebbesson. Approaching moisture recycling governance. *Global Environmental Change*, 45(April):15–23, 2017. ISSN 09593780. doi: 10.1016/j.gloenvcha.2017.04.007. URL https://doi.org/10.1016/j.gloenvcha.2017.04.007.

Patrick W. Keys, Lan Wang-Erlandsson, and Line J. Gordon. Megacity precipitationsheds reveal teleconnected water security challenges. *PLoS One*, 13(3):1–22, 2018. doi: https://doi.org/10.1371/journal.pone.0194311.

Patrick W. Keys, Miina Porkka, Lan Wang-Erlandsson, Ingo Fetzer, Tom Gleeson, and Line J. Gordon. Invisible water security: Moisture recycling and water resilience. *Water Security*, 8(May): 100046, 2019. ISSN 24683124. doi: 10.1016/j.wasec.2019.100046. URL https://doi.org/10.1016/j.wasec.2019.100046.

Jaya Khanna, David Medvigy, Stephan Fueglistaler, and Robert Walko. Regional dry-season climate changes due to three decades of Amazonian deforestation. *Nature Climate Change*, 7(3):200–204, 2017. ISSN 17586798. doi: 10.1038/nclimate3226.

Ryan Knox, Gautam Bisht, Jingfeng Wang, and Rafael Bras. Precipitation variability over the forest-to-nonforest transition in Southwestern Amazonia. *Journal of Climate*, 24(9):2368–2377, 2011. ISSN 08948755. doi: 10.1175/2010JCLI3815.1.

Deborah Lawrence and Karen Vandecar. Effects of tropical deforstation on climate and agriculture. 5(January), 2015. doi: 10.1038/NCLIMATE2430.

Argemiro T. Leite-Filho, Marcos H. Costa, and Rong Fu. The southern Amazon rainy season: The role of deforestation and its interactions with large-scale mechanisms. *International Journal of Climatology*, 40(4):2328–2341, 2019a. ISSN 10970088. doi: 10.1002/joc.6335.

Argemiro Teixeira Leite-Filho, Verônica Yameê de Sousa Pontes, and Marcos Heil Costa. Effects of Deforestation on the Onset of the Rainy Season and the Duration of Dry Spells in Southern Amazonia. *Journal of Geophysical Research: Atmospheres*, 124(10):5268–5281, 2019b. ISSN 21698996. doi: 10.1029/2018JD029537.

Brant Liebmann, Suzana J. Camargo, Anji Seth, José A. Marengo, Leila M.V. Carvalho, Dave Allured, Rong Fu, and Carolina S. Vera. Onset and end of the rainy season in South America in observations and the ECHAM 4.5 atmospheric general circulation model. *Journal of Climate*, 20(10): 2037–2050, 2007. ISSN 08948755. doi: 10.1175/JCLI4122.1.

Andreas Link, Ruud van der Ent, Markus Berger, Stephanie Eisner, and Matthias Finkbeiner. The fate of land evaporation - Basic dataset, 2019. URL https://doi.pangaea.de/10.1594/PANGAEA.908642.

Andreas Link, Ruud van der Ent, Markus Berger, Stephanie Eisner, and Matthias Finkbeiner. The fate of land evaporation – A global dataset. *Earth System Science Data Discussions*, 908705(January): 1–22, 2020. doi: 10.5194/essd-2019-246.

R. Lorenz, A. J. Pitman, and S. A. Sisson. Does Amazonian deforestation cause global effects; Can we be sure? *Journal of Geophysical Research*, 121(10):5567–5584, 2016. ISSN 21562202. doi: 10.1002/2015JD024357.

Yadvinder Malhi, J. Timmons Roberts, Richard A. Betts, Timothy J. Killeen, Wenhong Li, and Carlos A. Nobre. Climate change, deforestation, and the fate of the Amazon. *Science*, 319(5860): 169–172, 2008. ISSN 00368075. doi: 10.1126/science.1146961.

J. A. Marengo, B. Liebmann, V. E. Kousky, N. P. Filizola, and I. C. Wainer. Onset and end of the rainy season in the Brazilian Amazon Basin. *Journal of Climate*, 14(5):833–852, 2001. ISSN 08948755. doi: 10.1175/1520-0442(2001)014<0833:OAEOTR>2.0.CO;2.

Paulo Nobre, Marta Malagutti, Domingos F. Urbano, Roberto A.F. De Almeida, and Emanuel Giarolla. Amazon deforestation and climate change in a coupled model simulation. *Journal of Climate*, 22 (21):5686–5697, 2009. ISSN 08948755. doi: 10.1175/2009JCLI2757.1.

Jorge L. Peña-Arancibia, L. Adrian Bruijnzeel, Mark Mulligan, and Albert I.J.M. van Dijk. Forests as 'sponges' and 'pumps': Assessing the impact of deforestation on dry-season flows across the tropics. *Journal of Hydrology*, 574(December 2018):946–963, 2019. ISSN 00221694. doi: 10.1016/j.jhydrol.2019.04.064. URL https://doi.org/10.1016/j.jhydrol.2019.04.064.

C.W. Runyan, P. D'Odorico, and D. Lawrence. Physical and biological feedbacks of deforestation, 2012.

Fredrick H.M. Semazzi and Yi Song. A GCM study of climate change induced by deforestation in Africa. *Climate Research*, 17(2 SPECIAL 8):169–182, 2001. ISSN 0936577X. doi: 10.3354/cr017169.

I.A. Shiklomanov and J.C. Rodda. World water resources at the beginning of the 21st century. International hydrology series. *Cambridge University Press, Cambridge*, 2003.

D. V. Spracklen and L. Garcia-Carreras. The impact of Amazonian deforestation on Amazon basin rainfall. *Geophysical Research Letters*, 42(21):9546–9552, 2015. ISSN 19448007. doi: 10.1002/2015GL066063.

D. V. Spracklen, S. R. Arnold, and C. M. Taylor. Observations of increased tropical rainfall preceded by air passage over forests. *Nature*, 489(7415):282–285, 2012. ISSN 14764687. doi: 10.1038/nature11390.

Arie Staal, Bernardo M. Flores, Ana Paula D. Aguiar, Joyce H.C. Bosmans, Ingo Fetzer, and Obbe A. Tuinenburg. Feedback between drought and deforestation in the Amazon. *Environmental Research Letters*, 15(4):44024, 2020. ISSN 17489326. doi: 10.1088/1748-9326/ab738e. URL http://dx.doi.org/10.1088/1748-9326/ab738e.

Shannon M. Sterling, Agnès Ducharne, and Jan Polcher. The impact of global land-cover change on the terrestrial water cycle. *Nature Climate Change*, 3(4):385–390, 2013. ISSN 1758678X. doi: 10.1038/nclimate1690.

R. J. Van Der Ent, O. A. Tuinenburg, H. R. Knoche, H. Kunstmann, and H. H.G. Savenije. Should we use a simple or complex model for moisture recycling and atmospheric moisture tracking? *Hydrology and Earth System Sciences*, 17(12):4869–4884, 2013. ISSN 10275606. doi: 10.5194/hess-17-4869-2013.

R. J. van der Ent, L. Wang-Erlandsson, P. W. Keys, and H. H. G. Savenije. Contrasting roles of interception and transpiration in the hydrological cycle – Part 2: Moisture recycling. *Earth System Dynamics Discussions*, 5(1):281–326, 2014. ISSN 2190-4995. doi: 10.5194/esdd-5-281-2014.

Rudi J. Van Der Ent, Hubert H.G. Savenije, Bettina Schaefli, and Susan C. Steele-Dunne. Origin and fate of atmospheric moisture over continents. *Water Resources Research*, 46(9):1–12, 2010. ISSN 00431397. doi: 10.1029/2010WR009127.

Ruud J. Van Der Ent. *A new view on the hydrological cycle over continents (PhD thesis)*. PhD thesis, Delft University of Technology, 2014.

Lan Wang-Erlandsson, Ingo Fetzer, Patrick W. Keys, Ruud J. Van Der Ent, Hubert H.G. Savenije, and Line J. Gordon. Remote land use impacts on river flows through atmospheric teleconnections. *Hydrology and Earth System Sciences*, 22(8):4311–4328, 2018. ISSN 16077938. doi: 10.5194/hess-22-4311-2018.

Jiangfeng Wei and Paul A. Dirmeyer. Sensitivity of land precipitation to surface evapotranspiration: a nonlocal perspective based on water vapor transport. *Geophysical Research Letters*, 46(21):12588–12597, 2019. ISSN 19448007. doi: 10.1029/2019GL085613. URL https://doi.org/10.1029/2019GL085613.

David Werth and Roni Avissar. The local and global effects of Amazon deforestation, 2002.

Delphine Clara Zemp, Carl-friedrich Schleussner, Henrique M J Barbosa, Marina Hirota, Vincent Montade, Gilvan Sampaio, Arie Staal, Lan Wang-erlandsson, and Anja Rammig. Self-amplified Amazon forest loss due to vegetation-atmosphere feedbacks. *Nature Communications*, 2017. doi: 10.1038/ncomms14681.

L Zhang, W R Dawes, and G R Walker. Response of mean annual evapotranspiration to vegetation changes at catchment scale The research on the hydrological role of vegetation has. Technical Report 3, 2001. URL http://www.dist.gov.au/science/.